



## Hydrography of Northern Thermaikos Gulf based on an integrated observational-modeling approach

Y. Androulidakis<sup>a,b,\*</sup>, C. Makris<sup>a</sup>, V. Kolovoyiannis<sup>b</sup>, Y. Krestenitis<sup>a</sup>, V. Baltikas<sup>a</sup>, Z. Mallios<sup>c</sup>, I. Pytharoulis<sup>d</sup>, K. Topouzelis<sup>e</sup>, S. Spondylidis<sup>e</sup>, I. Tegoulis<sup>d</sup>, Y. Kontos<sup>c</sup>

<sup>a</sup> Laboratory of Maritime Engineering and Maritime Works, School of Civil Engineering, Aristotle University of Thessaloniki, Greece

<sup>b</sup> Laboratory of Physical and Chemical Oceanography, Department of Marine Sciences, University of the Aegean, Greece

<sup>c</sup> Laboratory of Water Resources Engineering and Management, School of Civil Engineering, Aristotle University of Thessaloniki, Greece

<sup>d</sup> Department of Meteorology and Climatology, School of Geology, Aristotle University of Thessaloniki, Greece

<sup>e</sup> Laboratory of Environmental Quality and Geospatial Applications, Department of Marine Sciences, University of the Aegean, Greece

### ARTICLE INFO

#### Keywords:

In situ observations  
 Drifters  
 Hydrodynamic circulation  
 Physical connectivity  
 Vertical structure  
 Delft3D

### ABSTRACT

The Northern Thermaikos Gulf is a semi-enclosed coastal region of the Aegean Sea, characterized by anthropogenic and natural stresses such as intense industrial and agricultural activities, urban outflows, and several river discharges facing severe pollution events. The main motivation of this study is to investigate the prevailing oceanographic conditions of Northern Thermaikos Gulf, which are associated with the quality of the semi-enclosed basin's water masses. The hydrography and the hydrodynamic circulation patterns are revisited, based on the findings of a multi-platform observational study, conducted during a recent annual cycle, from June 2021 until May 2022. The observational findings are supported by a three-dimensional high-resolution hydrodynamic model (Delft3D-Thermaikos) with updated freshwater input from all important land sources. The physical connectivity between the sub-basins of Thermaikos, the renewal of its northern coastal areas and the seawater quality are strongly related to the variability of wind-induced circulation. Northerly and southerly winds affect the spreading of the nutrient-rich riverine waters, discharged at the west coast of the gulf. The prevailing northerly winds contribute to the southward removal of the polluted sea surface and riverine waters, enhancing the cyclonic circulation around the gulf, allowing the inflow of clearer Aegean Sea Waters along the eastern coasts of the gulf. Northerlies also promote a connectivity pathway between the environmentally stressed Thessaloniki Bay (urban seafront) and the commonly less polluted southeastern coasts of the central basin. Southerlies mainly confine riverine waters in the western and northern coastal regions, weaken the renewal ability of the enclosed basins, and impose the formation of anticyclonic, mesoscale, circulation eddies in the outer and central areas.

### 1. Introduction

The Northern Thermaikos Gulf (NTG) is a semi-enclosed coastal basin, located at the edge of the northwestern Aegean Sea (eastern Mediterranean Sea; Fig. 1a). The metropolitan area of Thessaloniki, the second largest city in Greece with a population of 1.1 million inhabitants, is located along the gulf's northern coast and the entire coastline hosts numerous human activities. Two large (Axios and Aliakmonas) and two smaller (Gallikos and Loudias) rivers (Fig. 1a) supply freshwater into the NTG along its western coast, containing large quantities of nutrients (Karageorgis et al., 2005). Several smaller

outflows (e.g., Halastra open channel network, Anthemountas river; Fig. 1a) periodically discharge overflowing waters, containing agricultural (drainage), urban (treated and untreated wastewater) and industrial (liquid chemicals and heavy metals) pollutants (Gotsis-Skretas and Frilligos, 1990; Balopoulos and Frilligos, 1994; Pagou et al., 2000). The main pollution pressure of NTG, related to these inputs, is eutrophication (Genitsaris et al., 2019). It is strongly controlled by the mesoscale circulation patterns and the renewal capability of the gulf (Androulidakis et al., 2021). The water quality varies among the NTG sub-basins, controlled by the discharge of pollutants along the surrounding coasts, the physical connectivity between coastal areas, and the exchanges with

\* Corresponding author. Laboratory of Maritime Engineering and Maritime Works, School of Civil Engineering, Aristotle University of Thessaloniki, Greece.  
 E-mail address: [iandroul@civil.auth.gr](mailto:iandroul@civil.auth.gr) (Y. Androulidakis).

clearer water masses from the northern Aegean Sea (Aegean Sea Waters: ASW). The renewal capacity of the gulf and the prevailing circulation pathways also control the levels of microplastic pollution, originated from shipping, urban, aquaculture and agriculture activities (Kermenidou et al., 2023).

NTG is a typical, microtidal, mid-latitude, Mediterranean, coastal aquatic system. Thus, wind-induced circulation, riverine freshwater input, and water mass exchanges with the open sea (Aegean Sea; Fig. 1b) through the NTG southern open boundary, determine the characteristics of the marine hydrography, the water column structure, and the regional hydrodynamic circulation (Hyder et al., 2002; Krestenitis et al., 2012; Androulidakis et al., 2021). Previous studies (e.g., Krestenitis et al., 2012) showed that during cold periods, characterized mainly by northerly winds, the general cyclonic circulation around the Aegean Sea (Zervakis and Georgopoulos, 2002; Androulidakis and Kourafalou, 2011) may expand along the NTG coasts both in the upper and deeper layers, moving waters from the bay through the south boundary. This circulation pattern is not usually evident in the northern parts of Thermaikos Gulf during warm periods, when southerly winds prevail (Hyder et al., 2002). NTG is also characterized by dense water formation events, that provide dense water masses, through cascading, into the deeper North Aegean (Estournel et al., 2005; Zervakis et al., 2005; Krestenitis et al., 2012), and coastal upwelling/downwelling processes along its coasts (Savvidis et al., 2019). The general hydrography of NTG has been reported in the past with intermittent measurements (Hyder et al., 2002; Krestenitis et al., 2012) and modeling approaches (Kourafalou et al., 2004; Androulidakis et al., 2021).

We extended these studies by implementing a systematic network of bimonthly field measurements (of physical properties and currents) over the period from June 2021 to May 2022. The scope of this study is to investigate the prevailing oceanographic conditions of NTG under various wind and river conditions, which are proven to be associated with the quality of the water masses (Androulidakis et al., 2021). The main goals are to describe the connectivity pathways between the

sub-regions of NTG, the variability of the water column stratification and to examine the environmental conditions that determine the renewal and, hence the water quality of the semi-enclosed basin. To address these goals, a network of seven measurement stations, and 11 drifter deployments (Fig. 1a) were employed covering the three main sub-basins of the gulf (inner-, central-, outer-Gulf; Fig. 1a), following the categorization made by Androulidakis et al. (2021). River discharge rates (measured and simulated), satellite data (ocean color), high-resolution simulated meteorological and ocean data are also used to support the interpretation of the results derived from the field campaigns.

## 2. Methods and data

### 2.1. Field observations

The monitoring period covered a full year from June 2021 to May 2022 with a two-monthly temporal step (six campaigns on six specific dates, Table 1). The *in situ* measurements were conducted on board a research vessel. They include temperature, salinity, and current velocities covering the entire seawater column at seven stations, representative of the three main sub-basins of NTG (Fig. 1a). The maximum measurement depth of each station, derived as an average of the six field campaigns, ranged between 15 m (e.g., SIW) in the inner-Gulf to more than 24.5 m in the outer-Gulf (e.g., SOE; Table 1).

Temperature and salinity were recorded with a Conductivity-Temperature-Depth (CTD; Seabird SBE 19plus) instrument (Fig. 1f). All raw data were processed with SBE Data Processing software. It should be noted that due to CTD malfunction during the June 2021 campaign, the respective physical parameters (temperature and conductivity) were measured manually at three depths (near-surface, mid-depth, near-bottom) with the Inolab Cond 720 (WTW™) instrument that carries a four-electrode-conductivity cell with a built-in temperature sensor (TetraCon 325 Probe). Furthermore, vertical distributions of

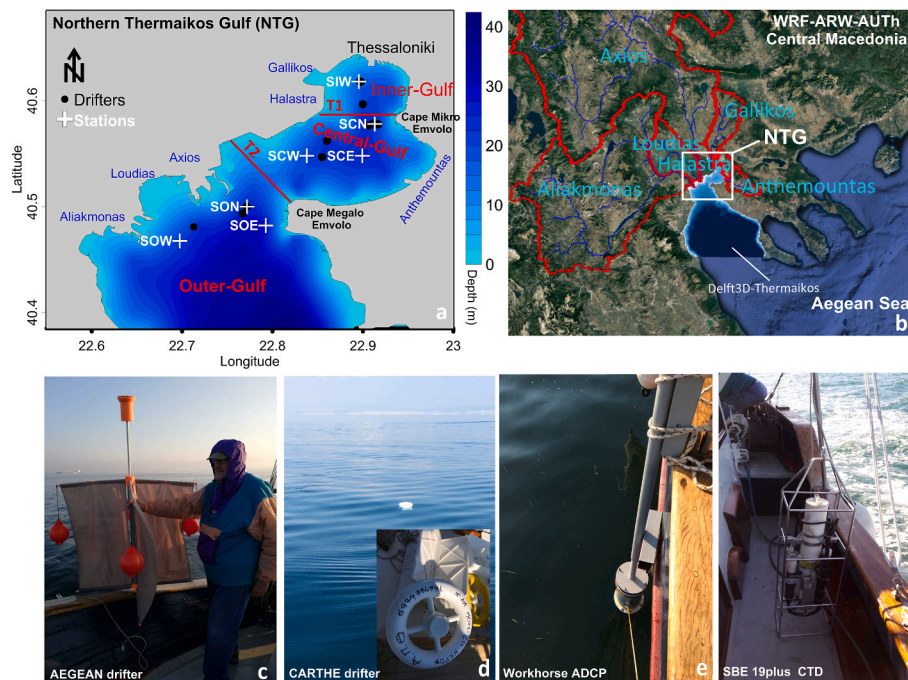


**Fig. 1.** (a) Northern Thermaikos Gulf bathymetry and the locations of seven stations (crosses; only ADCP data were collected in SCN for the last two campaigns) in the Inner-, Central-, and Outer-Gulf, divided by sections T1 and T2 (Androulidakis et al., 2021). Deployment locations of the 11 drifters are marked with black dots. (b) Domain of the WRF-ARW-AUTH model over the central Macedonia, river system (blue lines) that discharges into the NTG (white box), drainage river basins (inside red lines), and the Delft3D-Thermaikos model domain. Components of the observational platform: (c) "AEGEAN" drifter, (d) "CARTHE" drifter, (e) Workhorse ADCP, and (f) SBE 19plus CTD on board of R/V Poseidonia.

**Table 1**

Characteristics of the observational field data collected from June 2021 to May 2022. Temperature (T), Conductivity (C), ADCP current measurements (U).

| FIELD OBSERVATIONS (CTD, ADCP, DRIFTERS) |                       |                |   |              |               |   |   |
|--|-----------------------|----------------|---|--------------|---------------|---|---|
| Station                                  | SIW                   | SCW            | SON   | SOW          | SOE           | SCE   | SCN   |
| Location                                 | (Inner West)          | (Central West) | (Outer North)                                   | (Outer West) | (Outer East)  | (Central East)                                  | (Central North)                                   |
| Depth                                    | 15m                   | 20m            | 24m   | 24.5m        | 24.5m         | 24.5m   | 24m   |
| Date (dd.mm.yy)                          | 18.06.21 <sup>a</sup> | 31.08.21       | 29.10.21  |              | 04.01.22      | 18.03.22  | 10.05.22  |
| Station                                  |                       |                |   |              |               |   |   |
| SIW                                      | TC                    | TCU            | TCU   |              | TC            | TCU   | TCU   |
| SCW                                      | TC                    | TCU            | TCU   |              | TC            | TCU   | TCU   |
| SON                                      | TC                    | TCU            | TCU   |              | TC            | TC  | TCU   |
| SOW                                      | TCU                   | TCU            | TCU   |              | TC            | TC  | TC  |
| SOE                                      | TCU                   | TCU            | TCU   |              | TCU           | TCU   | TCU   |
| SCE                                      | TC                    | TC             | TC  |              | TCU           | TC  | TC  |
| SCN                                      | –                     | –              | –   |              | –             | U   | U   |
| Drifter (End Date)                       | D1 (19.06.21)         | –              | D2 (01.11.21)<br>D3 (01.11.21)<br>D4 (29.10.21) |              | D5 (04.01.21) | D6 (19.03.22)<br>D7 (26.03.22)<br>D8 (30.03.22) | D9 (12.05.22)<br>D10 (18.05.22)<br>D11 (18.05.22) |

<sup>a</sup> Profile measurements that do not cover the entire water column but only three depth levels (near-surface, mid-depth, near-bottom) due to CTD malfunction.

horizontal currents were also measured with the use of an Acoustic Doppler Current Profiler (ADCP; Workhorse Sentinel by TELEDYNE MARINE) in a moored mode at the same locations, providing temporal averages of approximately 20 min measurements at each station (Fig. 1e). The measured currents were post-processed by subtracting the (high-resolution GPS-track) recorded drift of the vessel during each ADCP deployment.

Near-surface circulation pathways were investigated with the deployment of 11 Lagrangian, autonomous, satellite-tracked, free-drifting floats (drifters) for the recording of ocean current velocities at different times and locations during the oceanographic campaigns (Table 1). Two types of drifters were used: i) eight AEGEAN drifters (Fig. 1c; Zervakis et al., 2009), developed by the Laboratory of Physical and Chemical Oceanography in the Department of Marine Sciences (University of the Aegean; <https://www.mar.aegean.gr/>), and ii) three CARTHE drifters (Fig. 1d), manufactured by the Consortium for Advanced Research on Transport of Hydrocarbon in the Environment (CARTHE; <http://carthe.org>; Novelli et al., 2017; Androulidakis et al., 2018). Durations of the drifter trajectories ranged from a few hours to several days and the time-interval of drifter location tracking varied

from 10 to 60 min. Almost half of the drifters (5) were recovered after the completion of the experiments at their coastal landing site or offshore due to battery drain.

## 2.2. River discharges

The main freshwater input to the NTG comes from four rivers (Gallikos, Axios, Loudias, and Aliakmonas) *in tandem* with a complex system of irrigation canals and drainage trenches (e.g., Halastra, Anthemountas; Fig. 1a). Measured daily outflow rates for the two larger rivers of Aliakmonas and Axios were provided by the Soil and Water Resources Institute (SWRI; Hellenic Agricultural Organization “DEMETER”; <https://www.swri.gr/>) and TERNA-ENERGY S.A. (<https://www.terna-energy.com/>), respectively. Daily discharges of the smaller rivers, canals and trenches were not available (Loudias, Gallikos, Halastra and Anthemountas). Therefore, the Hydrologic Modeling System (HEC-HMS; <https://www.hec.usace.army.mil/software/hec-hms/>) was implemented to simulate the hydrologic processes of the respective river basins that affect the NTG (Frysali et al., 2023). River outflows, measured and simulated (Fig. 2c), are an important piece of

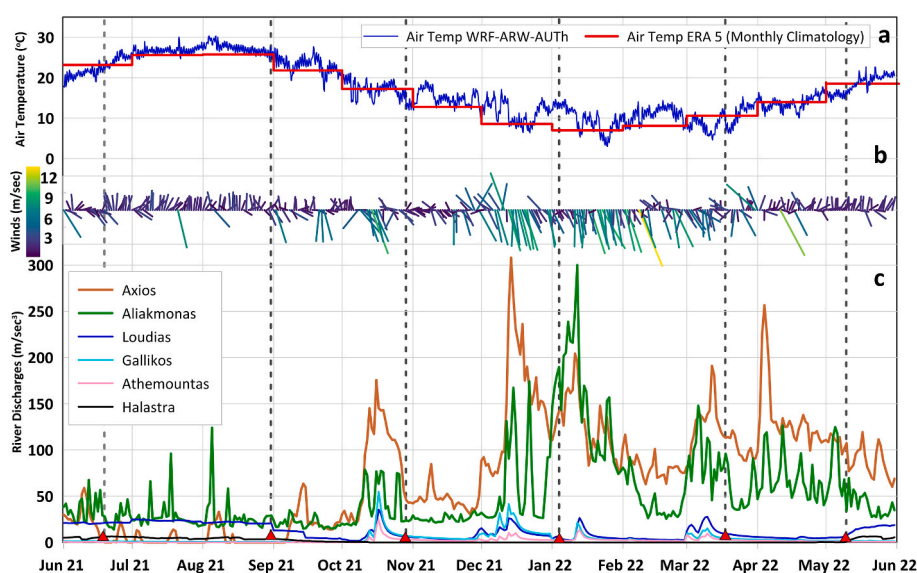


**Fig. 2.** Timeseries of (a) 3-hourly air temperature (°C; blue line), and (b) mean daily wind vectors (m/sec) from WRF-ARW meteorological simulations. The mean monthly climatology of air temperature from ERA5 reanalysis (1993–2021), averaged over the NTG is also shown in (a) (red line). (c) Axios, Aliakmonas, Loudias, and Gallikos rivers' daily discharge rates covering the study year (June 2021–May 2022). The 6 vertical dashed lines represent the dates of the field campaigns (Table 1).

information, as they play a determining role in the formation of the seawater column structure and the dynamics of the brackish water plumes. To this end, they are used as freshwater input in the numerical hydrodynamic simulations (Section 2.3).

### 2.3. Numerical simulations of meteorological and ocean conditions

The meteorological data (i.e., winds and air temperature), used for the analysis and as atmospheric input for the hydrodynamic simulations, were obtained from the operational system for met-ocean weather forecasts, Wave4Us (Krestenitis et al., 2014, 2015, 2017; <http://wave4us.web.auth.gr>). Simulations of regional-scale, high-resolution, atmospheric circulation were conducted with the Weather Research and Forecasting model's Advanced Research dynamic solver (Wang et al., 2010), developed in the Department of Meteorology and Climatology of the Aristotle University of Thessaloniki (WRF-ARW-AUTH; see Appendix). The simulations cover the broader Central Macedonia (Fig. 1b) that includes the Thermaikos Gulf with a 1.67 km × 1.67 km resolution (Table 2). We used the simulated 3-hourly air temperature (Fig. 2a) and wind (Fig. 2b) fields produced by the forecast system to examine the atmospheric effect on the circulation patterns and the distribution of the seawater's physical properties. The modeled fields of all the crucial atmospheric parameters were also used as forcing for the hydrodynamic simulations. In addition, the mean monthly climatology of air temperature over the Thermaikos Gulf (Fig. 2a) was also used to detect potential deviations in the meteorological conditions of the study year (June 2021–May 2022). It was computed from ERA5 hourly data on single levels from 1993 to 2021 with spatial resolution 0.25° × 0.25° (ECMWF re-analysis; Hersbach et al., 2018; <https://cds.climate.copernicus.eu/>; last accessed on 01/05/2023).

The ocean circulation conditions during 2021–2022 were reproduced by simulations with the Delft3D modeling system (Table 2), implemented over the broader Thermaikos Gulf (Delft3D-Thermaikos; Androulidakis et al., 2021, Fig. 1b). The model domain covers a wide area of the gulf (22.55–23.374°E and 39.96–40.643°N) and is defined by a 110 × 126 curvilinear grid, with a resolution step varying from approximately 750 m offshore near the open boundary (northwestern Aegean Sea) to less than 350 m in the inner-Gulf (Fig. 1b). Fifteen (15) sigma layers were used to vertically discretize the water column. The simulated current fields were firstly used to support the prevailing circulation patterns derived from the drifter experiments and current measurements and secondly to evaluate the transport and renewal processes of NTG. More detailed information about the numerical simulations (meteorological and hydrodynamic) during the 2021–2022 period and the validation of Delft3D-Thermaikos model are presented in Section 2 of the Appendix.

### 2.4. Satellite-derived data

The satellite data used in the study are derived from ocean color images that provide high-resolution estimations of chlorophyll-a (chl-a) concentrations for the surface, over the entire study region. All the

collected raw satellite images refer to Sentinel-2 and Sentinel-3 datasets, derived from EU's Earth Observation Programme platform, Copernicus (<https://www.copernicus.eu/>). The Sentinel-2 satellite has a spatial resolution of 10 m in Visible (RGB) and Near Infra-Red (NIR) bands and a revisit time of five days. For Sentinel-2 satellite, the Level-1C product was used. After pre-processing (atmospheric correction, land mask and cloud mask), the Case-2 Regional Coast Color (C2RCC; Brockmann et al., 2016) algorithm was applied to estimate chl-a concentrations utilising the SNAP-C2RCC toolbox. C2RCC uses a large database of radiative transfer simulations, inverted by neural networks, for the derivation of the chl-a concentration product. In addition, data were collected from Sentinel-3 satellite, i.e., the Ocean and Land Color Instrument (OLCI). OLCI uses optical bands to retrieve ocean images with 300 m spatial resolution on a daily basis. Chl-a concentrations from Sentinel-3/OLCI are a standard Level-2 product, derived from the OC4Me Chlorophyll algorithm (Morel et al., 2007; Kyriliuk and Kratzer, 2019). Both satellites (Sentinel-2 and Sentinel-3) were used to increase the temporal resolution; the Sentinel-3 (300 m resolution) for daily and Sentinel-2 (10 m resolution) for a five-days step chl-a estimation. Horizontal fields of chl-a concentrations during the study period were produced. The respective concentrations from all available images at the six measurement stations were also derived to detect potential blooms and eutrophication events, providing qualitative information about the quality of the water masses and their renewal level. The chl-a concentration may provide information about the quality state of the semi-enclosed sub-basins (Androulidakis et al., 2021). Moreover, chl-a concentration is a good indicator of nutrient-rich river plume spreading in NTG, especially over the outer-Gulf where the two large deltas (Axios and Aliakmonas) are located. However, there are cases that salinity, indicator of riverine/ocean waters, and chl-a can be positively correlated (e.g., freshwater influence at areas with low chl-a concentrations and the opposite). It should be noted that the algorithms used for the chl-a concentration estimation were not calibrated for the specific region and time window based on *in situ* measurements. This is important as these algorithms were not designed for application in oligotrophic areas, like the Aegean Sea, and as such they cannot accurately quantify chl-a concentrations (Moutzouris-Sidiris and Topouzelis, 2021). Nonetheless, these data can provide qualitative information on the general surface distribution of chl-a concentrations over the study area and enable the distinction between areas of high and low productivity associated to the renewal processes and the quality of water masses (Androulidakis et al., 2021).

## 3. Results

### 3.1. Observational and modeling fields during the 6 campaigns

The recorded vertical profiles of temperature, salinity, and density, derived from all measurements (six campaigns at six stations) and the satellite-derived chl-a concentrations, are presented in Figs. 3 and 4. The respective wind and near-surface circulation conditions during the six campaigns are described based on simulated winds, modeled currents,

**Table 2**

Main characteristics of the hydrological, atmospheric, and hydrodynamic, numerical simulations. Note that Axios and Aliakmonas discharges were derived from field measurements.

|                                | SIMULATIONS                               |  |                          |   |
|--------------------------------|---|--|--------------------------|---|
|                                | HYDROLOGIC                                |  | ATMOSPHERIC              | HYDRODYNAMIC  |
| <b>Model</b>                   | HEC-HMS                                   | Measurements<br>TERNA-ENERGY S.A. & ELGO DEMETER | WRF-ARW-AUTH             | Delft3D-Thermaikos                                    |
| <b>Domain &amp; Resolution</b> | Loudias, Gallikos, Halastra, Anthemountas | Axios, Aliakmonas                                | Central Macedonia 1670 m | North Thermaikos Gulf<br>350–750 m<br>15 sigma layers |
| <b>Temporal</b>                | Daily data                                |  | 3-hourly data            | 3-hourly data   |
| <b>Output</b>                  | Discharge rates (m <sup>3</sup> /sec)     |  | Air temperature, winds   | Temperature, Salinity, Currents                       |

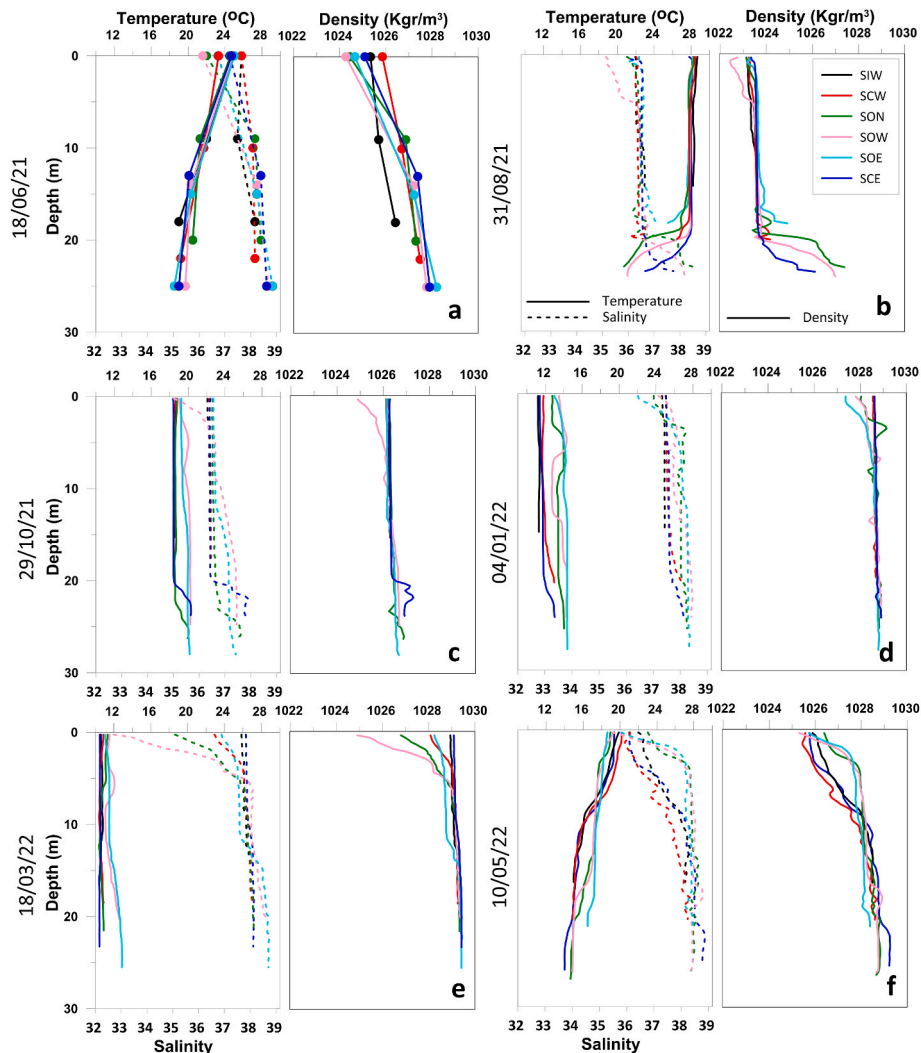


**Fig. 3.** Vertical distribution of temperature (solid lines), salinity (dashed lines), and density (solid lines), for each station during (a) 18 June 2021 (19 June for S1), (b) 31 August 2021, (c) 29 October 2021, (d) 04 January 2022, (e) 18 March 2022, and (f) 10 May 2022 campaign. Measurements were collected only at three depths (dots) in June (graph panel a; see also Table 1).

drifter trajectories, and ADCP measurements.

### 3.1.1. June conditions

The low outflow rates of all rivers in June ( $<60 \text{ m}^3/\text{s}$ ; Fig. 2c) mainly affected the surface salinity levels (around 36) of Stations SON and SOW, located in the vicinity of the large deltas of Axios and Aliakmonas, respectively (Fig. 3a). The water column at all stations was stratified with lower densities at the surface ( $1024\text{--}1025 \text{ kg}/\text{m}^3$ ) and higher values near the bottom ( $1027\text{--}1028 \text{ kg}/\text{m}^3$ ). Northwestern winds prevailed during the previous period (Fig. 2b) contributing on the southward removal of surface waters that reduced the chl-a concentrations at all stations ( $<2 \text{ mg}/\text{m}^3$ ; Fig. 4a and b). The dominance of northerly winds supports the renewal of the enclosed basins and reduces the chl-a values (see Section 3.3). Androulidakis et al. (2021) showed that apart from the favourable biological conditions (Genitsaris et al., 2019), wind conditions that control the circulation and renewal of the NTG, may also control the chl-a levels of the gulf. However, the southerly winds ( $>6 \text{ m/s}$ ) that prevailed in the afternoon of 18/06 induced a strong northeastward flow, as measured at Stations SOW and SOE ( $>0.3 \text{ m/s}$ ) and derived by the numerical hydrodynamic simulation (18/06 15:00; Fig. 5a). Strong northeastward currents mainly formed along the western coasts of the outer-Gulf (Fig. 5a). This northeastward coastal current, explains the detection of low-density water masses ( $1024.2$

$\text{kg}/\text{m}^3$ ; Fig. 3a) at the surface of Stations SOW and SON, both being affected by the less saline river plume (Salinity: 36) that was restricted along the western coasts of the gulf.

Northeastward currents were also detected along the western coasts of the central-Gulf (Fig. 5a). They were part of a clear anticyclonic eddy over the entire central basin. The spreading of waters over the central-Gulf, controlled by the southerly winds, was also confirmed by the trajectory of Drifter D1 that moved northeastward and got trapped inside the anticyclonic eddy (Fig. 5a). The short-term reversal of the winds from southerlies to northerlies on 19/06 (one day after the drifter deployment and the *in situ* measurements) weakened the anticyclonic circulation of the central-Gulf. It further imposed strong southward currents ( $\sim 0.25 \text{ m/s}$ ) over the western inner-Gulf, connecting it with the central-Gulf. High salinity (37.8; Fig. 3a) was measured at the shallow Station SIW of the inner-Gulf in the morning of 19/06.

### 3.1.2. August conditions

Southerly winds, but of slightly higher magnitude ( $\sim 8 \text{ m/s}$ ) compared to the June campaign, prevailed during the field campaign on 31/08 (Fig. 5b). Note that drifter experiments were not executed during this campaign (Table 1). A clear anticyclonic eddy also formed in the central-Gulf. The eddy was more profound in the evening (31/08 18:00; Fig. 5b) when stronger winds occurred, forming alongshore currents in

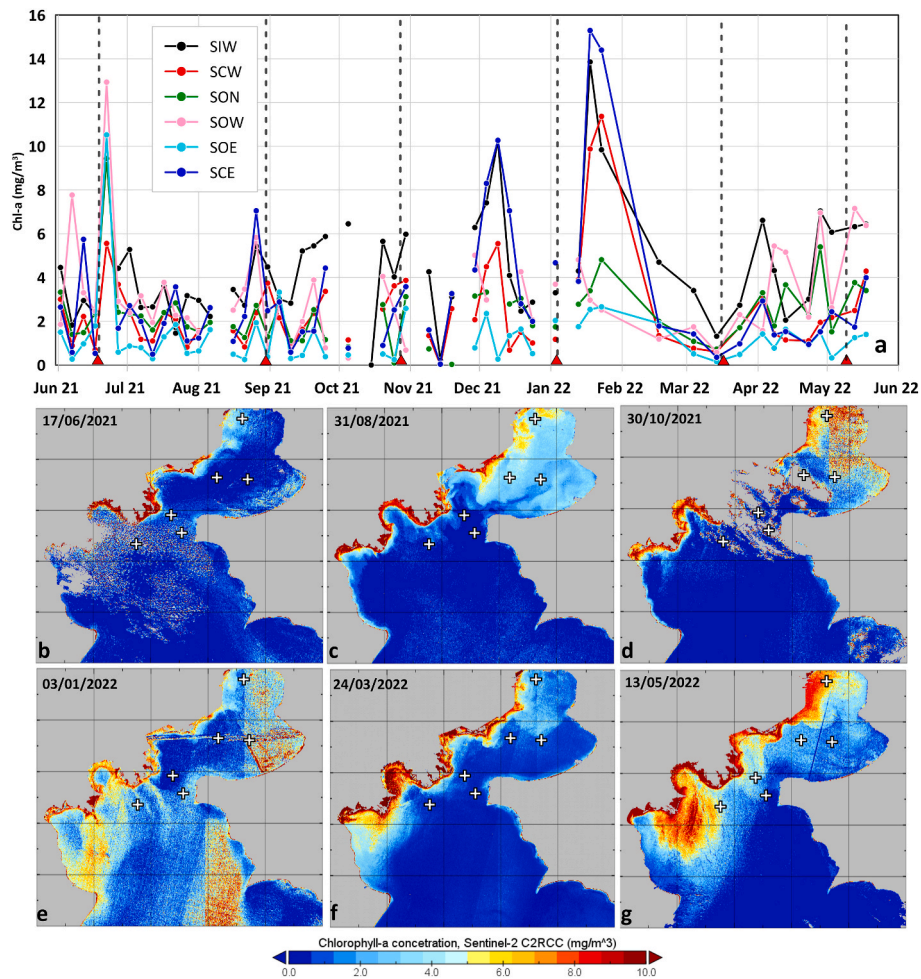


**Fig. 4.** (a) Depiction of chl-a concentrations ( $\text{mg}/\text{m}^3$ ) around the locations of the 6 stations (crosses on maps), derived from available satellite ocean colour images covering the annual study period (June 2021–May 2022). Horizontal distributions of the chl-a concentrations, derived from 6 available ocean color images, the closest possible to the 6 campaign dates, are presented for (b) June, (c) August, (d) October, (e) January, (f) March, and (g) May. The 6 vertical dashed lines (in graph a) represent the dates of the field campaigns (Table 1).

the western central-Gulf. The intense alongshore flow was also confirmed by the measured currents at all stations located along the western coasts. Stronger magnitude was recorded at Station SCW that captured the western boundary of the central-Gulf's anticyclonic eddy ( $0.25 \text{ m/s}$ ; Fig. 5b). The northeastward flow, and especially the dominance of high temperature levels reduced the density values ( $<1023.5 \text{ kg}/\text{m}^3$ ; Fig. 3b) over the entire NTG. The lowest salinity values were detected in the western outer-Gulf (Station SOW; Fig. 3b). This was due to the confinement of brackish waters, associated to the northward currents that were measured in the upper layers (Station SOW) in agreement with the simulated surface currents (Fig. 5b). The eastern part of the outer-Gulf was characterized by southeastward currents in the morning of 31/08 (Fig. 5b) with strong velocities near the surface ( $0.25 \text{ m/s}$ ) due to the formation of a second anticyclonic eddy over the outer-Gulf. A respective chl-a peak in the inner- and central-areas was observed in late-August ( $5.5\text{--}7 \text{ mg}/\text{m}^3$ ; Fig. 4c), when less-favourable renewal conditions, associated with the southerly winds, prevailed (see Section 3.3).

Very warm waters ( $>28^\circ\text{C}$ ) were observed at the upper 15 m of all stations. The high temperature values were probably related to the intense Marine Heat Wave (MHW) events that occurred over the entire Thermaikos Gulf due to the high atmospheric temperatures (exceeding the decadal monthly mean) (Fig. 2a) of August 2021 (see Section 4.1; Androulidakis and Krestenitis, 2022). The density gradient was large only in Station SOW due to the subsurface halocline and at the

near-bottom layers of Stations SON, SOW and SCE where colder and saltier waters were observed (Fig. 3b). The deeper ( $>20 \text{ m}$ ) outer-Gulf (Stations SON, SOW and SOE) and the eastern central-Gulf (Station SCE) were occupied by denser open sea waters ( $1025\text{--}1027.5 \text{ kg}/\text{m}^3$ ), originated from the Aegean Sea (ASW; see Section 3.3). The ASW mass was not present in the shallower inner-Gulf (Station SIW), which revealed lower density values and a more homogenous water column (Fig. 3b). The near-bottom simulated currents (not shown) are characterized by a northward flow that spread from the outer-Gulf to the northern parts of the central-Gulf without entering in the inner-Gulf. The reversal of winds to northerlies in the morning of 01/09 weakened the anticyclonic circulation in the central-Gulf and formed a clear connectivity pathway from the inner- and central-to the outer-Gulf, similar to 19/06 (Fig. 5b). The removal of surface waters towards the South that promoted the renewal of the NTG (see Section 3.3), quickly reduced the chl-a concentrations to less than  $4 \text{ mg}/\text{m}^3$  in the beginning of September (Fig. 4a).

### 3.1.3. October conditions

The mid-autumn (29/10) conditions were characterized by weaker winds ( $<4 \text{ m/s}$ ) and very low current velocities ( $<0.1 \text{ m/s}$ ; Fig. 6a), while the water column was homogenous in almost all areas (Fig. 3c). The majority of the *in situ* seawater density records showed values between  $1026$  and  $1027 \text{ kg}/\text{m}^3$ .

Strong northward current velocities were only measured and

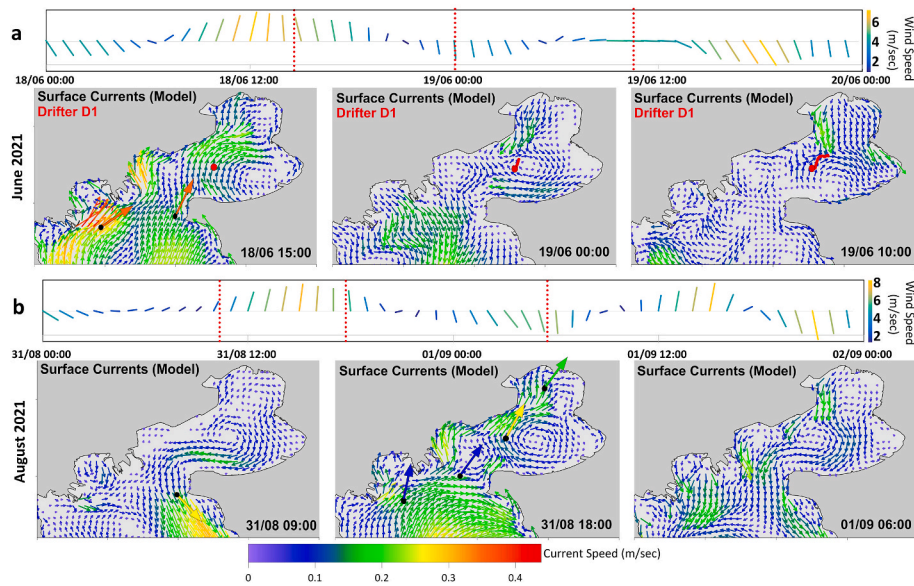


**Fig. 5.** Characteristic snapshots of drifter’s trajectory (D1) and ADCP surface (0–1 m) currents (large vectors) overlaid on respective simulated (Delft3D-Thermaikos, surface layer) currents during (a) June 2021, and (b) August 2021 campaigns. Timeseries of wind vectors derived from the WRF-ARW-AUTH simulations (at Station SCW) during the drifter periods are presented for each case (dashed red lines mark the dates of the horizontal maps). The ADCP current vectors are placed in the snapshot with the nearest respective date/hour to the measurement.

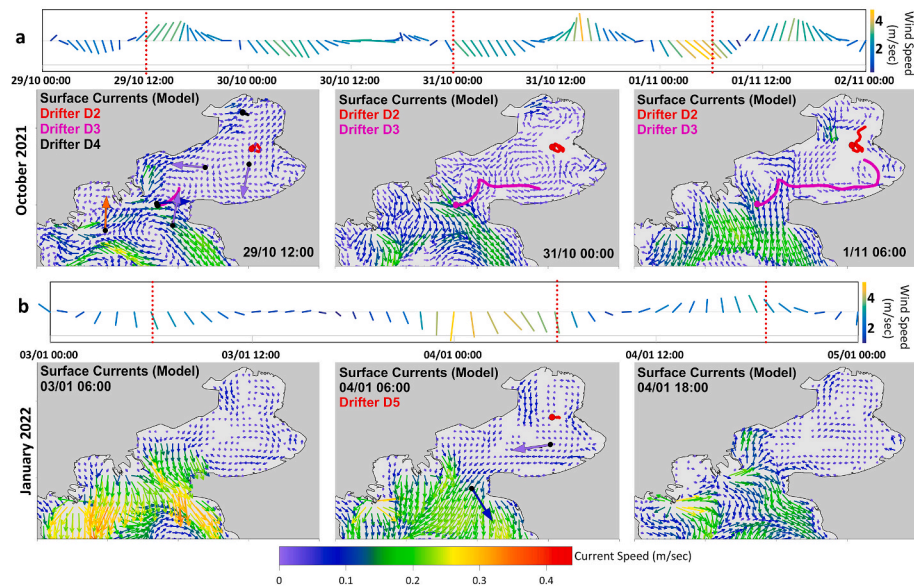


**Fig. 6.** Characteristic snapshots of drifters’ trajectories (D2, D3, D4, D5) and ADCP surface (0–1 m) currents overlaid on respective simulated (Delft3D-Thermaikos, surface layer) currents during (a) October 2021 and (b) January 2022 campaigns. Timeseries of wind vectors derived from the WRF-ARW-AUTH simulations (at Station SCN for October and at Station SCW for January) during the drifter periods are presented for each case (dashed red lines mark the dates of the horizontal maps). The ADCP current vectors are placed in the snapshot with the nearest respective date/hour to the measurement.

simulated in the outer-Gulf (e.g., Station SOW Fig. 6a). The northward flow in the western outer-Gulf, related to the weak southwesterly winds on 29/10 (<4 m/s; Fig. 6a), formed an anticyclonic eddy that covered the northern outer-Gulf. Besides SOW (northward), this eddy was also evident in the surface current measurements at Station SON (eastward). The temperature of the central- and inner-Gulf was around 18.5 °C, while the water masses of the outer-Gulf (Stations SOW and SOE; Fig. 3c) were warmer (>19 °C). A low salinity (35) water mass was only detected at the surface of the western outer-Gulf (Station SOW; Fig. 3c) related to the strong Axios discharges (>150 m<sup>3</sup>/s; Fig. 2c) and the strong northerly winds and (Fig. 2b) during the previous period, in mid-October, that pushed the river plume southward. The confined brackish

waters over this southwestern region caused the induction of a weak stratification peak (halocline) over the upper 5 m layer of Station SOW (Fig. 3c). The eastward spreading of waters induced by the anticyclone in the outer-Gulf, was also apparent in the motion of Drifter D3, deployed at Station SON on 29/10 (Fig. 6a). D3 was advected eastwards moving at the outermost periphery of the anticyclone. The southerly winds enhanced the northward spreading of surface waters across the western entrance of the central-Gulf and along the coasts until 30/10. A few hours after its deployment, in the evening of 29/10, Drifter D3 “escaped” from the eddy and entered the central-Gulf, where it was entrapped in a cyclonic pattern after 31/10. This cyclonic eddy moved Drifter D3 eastward, along the eastern coasts (eastern boundary of the

eddy; Fig. 6a).

The northern part of the central-Gulf was generally characterized by very weak currents ( $<0.02$  m/s) resulting to a short Drifter D2 trajectory, mainly around its deployment area in the eastern entrance of the inner-Gulf (Station SCN; Fig. 6a). The southwesterly winds on 29/10 slowly advected Drifter D4 eastward in the inner-Gulf for a few hours before its recovery at the same day (Fig. 6a). A weak anticyclonic circulation was formed in the inner-Gulf during the following days under northerly winds (31/10). It is shown that southerly winds may drag surface waters from the vicinity of Axios delta eastward under anticyclonic circulation in the northern outer-Gulf and directly into the central-Gulf along the western coasts (29/10). Northwesterly winds, which were dominant direction-wise over Thermaikos Gulf on 30–31/10 (Fig. 5a), may enhance the cyclonic circulation in the central-Gulf and spread the surface waters anticlockwise, around the coasts of the central sub-basin.

### 3.1.4. January conditions

The water column was homogenous ( $>1028$  kg/m<sup>3</sup>; Fig. 3d) in early-January with relatively high salinity values ( $>37$ ) over almost the entire NTG. The water column temperature was around 11 °C for the inner- (Station SIW) and central-Gulf (Stations SCW and SCE) resulting to very high values of density ( $>1028.5$  kg/m<sup>3</sup>). On the contrary, warmer waters were detected in the entire water column of the outer-Gulf (13–14 °C). Only the upper layers of the outer-Gulf (Stations SON, SOW and SOE; Fig. 3d) showed any stratification (high density gradients) related to the southward spreading of riverine waters under northerly winds (Fig. 6b). Strong northerly winds prevailed over NTG during the second half of December (Fig. 2b). They contributed to the southward removal of the surface waters and enhanced the renewal of the gulf (see Section 3.3). The brackish plume was absent in the central and northern parts of the gulf, although the river discharge rates were significantly high during the previous period (120–300 m<sup>3</sup>/s; Fig. 2c). A near-surface water mass with lower salinity was detected at the central and eastern parts of the outer-Gulf (Stations SON and SOE; Fig. 3d), related to the offshore southward spreading of brackish waters (Fig. 6b). The discharges were reduced by the end of December, increasing the salinity levels ( $>37$ ) in the vicinity of the river deltas (western part of the Gulf; Stations SON and SOW; Fig. 3d).

Weak northerly and westerly winds prevailed in the morning of the field campaign (Fig. 6b) pushing Drifter D5 eastward after its deployment in Station SCN early in the morning. The respective surface currents over the central- (Station SCE) and especially in the outer-Gulf (Station SOE) are characterized by a southward component linked to even stronger northerly winds that prevailed over the outer-Gulf (not shown). The simulated currents agree with the observed surface flows, where an extended southward surface flow was computed, especially over the outer-Gulf. The southward spreading of surface waters also reduced the chl-a concentrations at the end of December and early-January (Fig. 4a). On the contrary, the prevalence of stronger southerly winds ( $>10$  m/s; Fig. 2b) during the first half of December spread surface waters at all gulf's sub-basins and weakened the renewal of the enclosed basins (see Section 3.3) increasing the chl-a concentrations (Fig. 4a). It is noted that during the same period the nutrient-rich river outflows were significantly high (e.g.,  $>300$  m<sup>3</sup>/s for Axios,  $>150$  m<sup>3</sup>/s for Aliakmonas, and  $\sim 50$  m<sup>3</sup>/s for Gallikos; Fig. 2c).

### 3.1.5. March conditions

The temperature levels further decreased until the mid-March campaign, when temperature above 12 °C was only detected in the deeper layers of the outer-Gulf (Stations SOW and SOE; Fig. 3e). The central- (SCE) and inner-Gulf (SIW) basins were occupied by masses with very low temperature ( $\sim 11$  °C) and high salinity (38), increasing density to 1029 kg/m<sup>3</sup> in the entire water column (Fig. 3e). The low air temperature conditions in March, colder than the monthly climatological mean (Fig. 2a), combined with the intense wind-induced mixing of

the previous months under strong northerlies (prolonged periods with the highest annual magnitudes from January to March 2022; Fig. 2b), contributed to the cooling down of the water masses of the entire NTG.

In mid-March, southeastward and northward currents were measured in the surface of Station SIW and SCN, respectively, linked to the cyclonic circulation in the inner-Gulf under southerly winds (18/03) in agreement with the simulated currents (Fig. 7). The cyclonic circulation in the inner-Gulf also determined the trajectory of Drifter D7 that was deployed at Station SCN in the morning of the field campaign. The cyclonic circulation was still apparent until 21/03 00:00 when Drifter D7 reached the northwest tip of the inner-Gulf. Drifter D6 was also deployed in the evening of 18/03 and confirmed the same pattern until 20/03.

Eastward near-surface currents were measured in Station SCW (0.3 m/s), confirming the formation of a strong anticyclonic eddy in the central-Gulf under the same wind conditions (Fig. 7). The northeastward boundary of the anticyclonic circulation in the western central-Gulf explains the river plume spreading along the western coast that reduced near-surface salinity in Stations SON and SCW (Fig. 3e). The vertical structure of the water column was characterized by strong stratification only in the upper layers of the western and southern stations (SCW, SON, SOW and SOE; Fig. 3e), associated with the high discharge rates and (100–180 m<sup>3</sup>/s during March 2022; Fig. 2c) the anticyclonic circulation. The river plume reduced the salinity below 33 in Station SOW, around 35 in Station SON and below 37 in Station SCW. High chl-a concentrations were observed only in the vicinity of the river discharges, along the western coast (Fig. 4f) while the concentration at all stations was significantly low ( $<2$  mg/m<sup>3</sup>; Fig. 4a). Saltier waters ( $>38.5$ ) occupied the deeper layers of the outer-Gulf (Stations SOW and SOE; Fig. 3e). The southerly winds formed another anticyclonic eddy over the northern part of the outer-Gulf (Fig. 7), similar to the circulation conditions detected in June (Fig. 5a), August (Fig. 5b), and October (Fig. 6a). Drifter D8 (Fig. 7) was deployed in the vicinity of the deltas (Station SOW) on 18/03 and rapidly moved eastward towards Station SOE, following this anticyclonic pattern. The eastward spreading of the brackish waters, detected in the eastern outer-Gulf, is responsible for the halocline of 1 m in the upper 5 m at Station SOE (Fig. 3e).

The anticyclonic circulation of the central-Gulf that was formed under southerly winds (18–19/03) was significantly weakened under northerlies (20–25/03), replaced by a southward spreading of waters along the western coasts of the central-Gulf and over the entire outer-Gulf. The dominance of northerly winds induced a strong southward flow along the western coasts and towards the central-Gulf that pushed Drifter D7 southward from 21/3 until 26/3 establishing a southward connectivity pathway between the northern coasts and the eastern coasts of the central-Gulf. Drifter 7 completed a full circle over the inner- and central-Gulf during a 9-day period. The dominance of northerly winds (10 m/s) during the following days also promoted a clear southward removal of surface waters over the entire outer-Gulf, with very strong velocities ( $>0.4$  m/s) as shown in both simulated currents and Drifter D8 trajectory (Fig. 7). The southward pathway of Drifter D8 continued until the end of the month under weaker winds of both southward and northward directions that also pushed the drifter offshore (30/3 00:00; Fig. 7).

### 3.1.6. May conditions

Towards the end of spring (10–18/05; Fig. 8), strong southerly winds prevailed over the NTG, with short-term reversals to northerlies in the morning of each day. The temperature levels, measured on 10/05, were between 14 °C to 20 °C, with higher salinities than in March (36–39 from surface to the bottom; Fig. 3f). Stratified water columns were detected in all areas with a large range of density values (1025–1029 kg/m<sup>3</sup>) and a pronounced pycnocline in the upper 10 m, associated with the north-eastward currents that prevailed over NTG under southerly winds, especially along the western coasts, where the main freshwater sources are located (Fig. 7) The near-surface water masses were characterized by

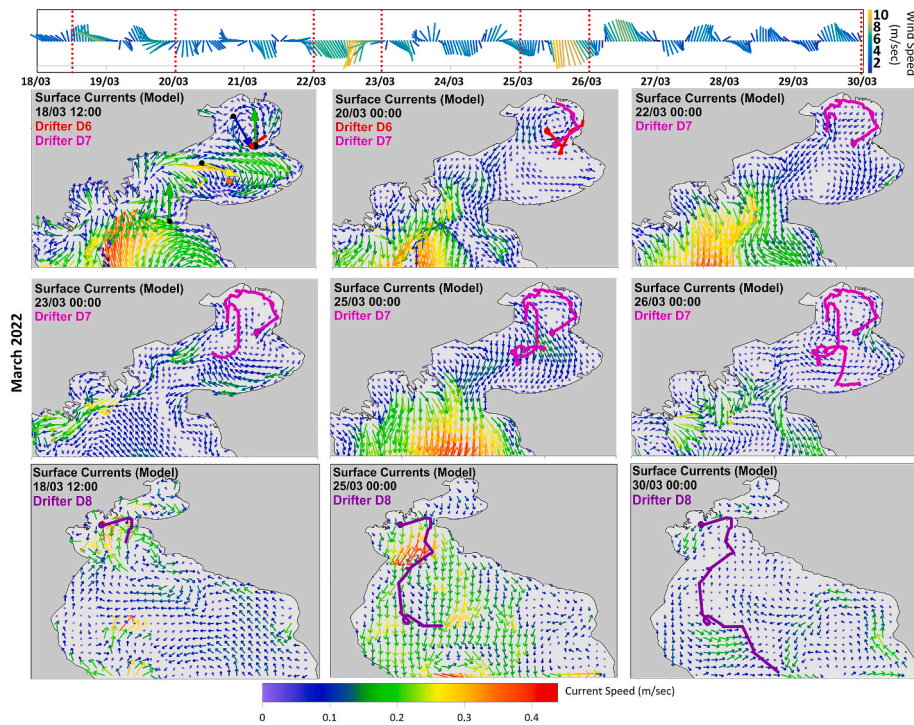


**Fig. 7.** Characteristic snapshots of drifters’ trajectories (D6, D7, D8) overlaid on respective simulated (Delft3D-Thermaikos, surface layer) currents during March 2022 campaign. Timeseries of wind vectors derived from the WRF-ARW-AUTH simulations (at Station SCN) during the drifter periods are presented for each case (dashed red lines mark the dates of the horizontal maps). The ADCP current vectors are placed in the snapshot with the nearest respective date/hour to the measurement.

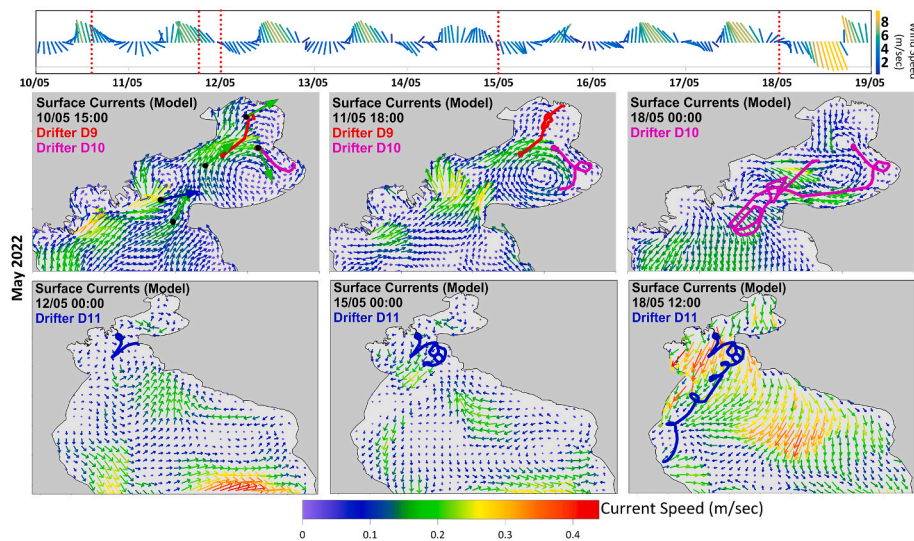


**Fig. 8.** Characteristic snapshots of drifters’ trajectories (D9, D10, D11) and ADCP surface (0–1 m) currents overlaid on respective simulated (Delft3D-Thermaikos, surface layer) currents during May 2022 campaign. Timeseries of wind vectors derived from the WRF-ARW-AUTH simulations (at Station SOE) during the drifter periods are presented for each case (dashed red lines mark the dates of the horizontal maps). The ADCP current vectors are placed in the snapshot with the nearest respective date/hour to the measurement.

increased chl-a concentrations ( $>5 \text{ mg/m}^3$ ; Fig. 4a), associated with the weak but continuous southerly winds that might have weakened the renewal capability of the area (Fig. 2b). Relatively large quantities of nutrient-rich waters had been discharged in the gulf by Axios and Aliakmonas a few days before the campaign ( $>100 \text{ m}^3/\text{s}$ ; Fig. 2c).

The southerly winds formed an anticyclonic eddy that evolved in the central-Gulf for several days (10–18/05; Fig. 8). Current measurements at Stations SCN and SCW confirm the presence of the anticyclonic eddy on 10/05; the eastward component of the currents at Station SCW

represented the northern boundary of the eddy, while the eastern boundary of the anticyclone (Station SCN) was characterized of southward currents (Fig. 8). Drifter D10 was deployed in the northern central-Gulf (Station SCN) in the morning of 10/05 (Fig. 8) and followed a southeastward pathway towards the eastern coasts, along the periphery of the anticyclone. The drifter turned towards the west reaching the southern exit of the central-Gulf on 15/05, when northerly winds formed southward currents over the outer-Gulf. The successive reversal of the winds from northerlies to southerlies and the respective change of

the current direction between 15/05 and 16/05 promoted two clockwise circles of the drifter, which finally entered the central-Gulf where it was entrained in the anticyclonic eddy that was still over the area. Drifter D9 was deployed in the opposite side of the central-Gulf in the afternoon of 10/05 and moved northward by the same anticyclonic eddy (Fig. 8). It quickly reached the northern coasts of the Gulf revealing a strong connectivity pathway between the central- and inner-Gulf along the western coasts in agreement with the northeastward currents (0.2 m/s), measured in Stations SCW (western central-Gulf) and SIW (inner-Gulf).

The anticyclonic circulation that was observed over the northern outer-Gulf in March (recorded by Drifter D8; Fig. 7) was again present in May forming successive circles of Drifter D11 after its deployment at Station SOW on 10/05 (Fig. 8). The drifter remained over this area for 3 days. Increased stratification was detected in the upper layers of Stations SON, SOW and SOE (outer-Gulf). A very strong halocline ( $>3$ ) formed over the upper 5 m layer of this area with salinity reaching approximately 35.5 near the surface and exceeding 38 at the deeper part of the water column, which was mainly affected by ASW. This dense water mass was also tracked in the deeper layers of the central-Gulf (Station SCE; Fig. 3f). Finally, the northerly winds that prevailed in the beginning of each day moved the drifter further southward under strong near-surface currents ( $>0.30$  m/s), revealing however small scale inertial

clockwise rotations after the semidiurnal change of the winds from northerlies to southerlies. The overall pathway connected the outer part of the NTG (vicinity of river deltas and exchange area between outer- and central-Gulf) with the southwestern coasts of the broader Thermaikos Gulf. Drifter D11 covered a long distance of approximately 50 km in less than 3.5 days (15/5–18/5; Fig. 8) showing a mean translation speed of 0.20 m/s.

### 3.2. Analysis of relative vorticity variability

The Relative Vorticity (RV) fields, normalized by the Coriolis frequency  $f$  ( $RV/f$ ), were derived from the 3-hourly simulated currents of the model's surface layer for the entire study period (June 2021–May 2022; Fig. 9) to quantify the variability of the mesoscale near-surface circulation patterns. The  $RV/f$  was averaged over the inner- and central-Gulf of the NTG (Fig. 1a) and is discussed together with the wind variability derived at section T1 (Fig. 1a) that divides the two sub-basins. It is noted that besides the wind-driven circulation, which is the most important factor in this semi-enclosed basin, the hydrodynamic circulation of the NTG is also determined by other environmental conditions such as the river plume dynamics and the exchanges with the open sea.

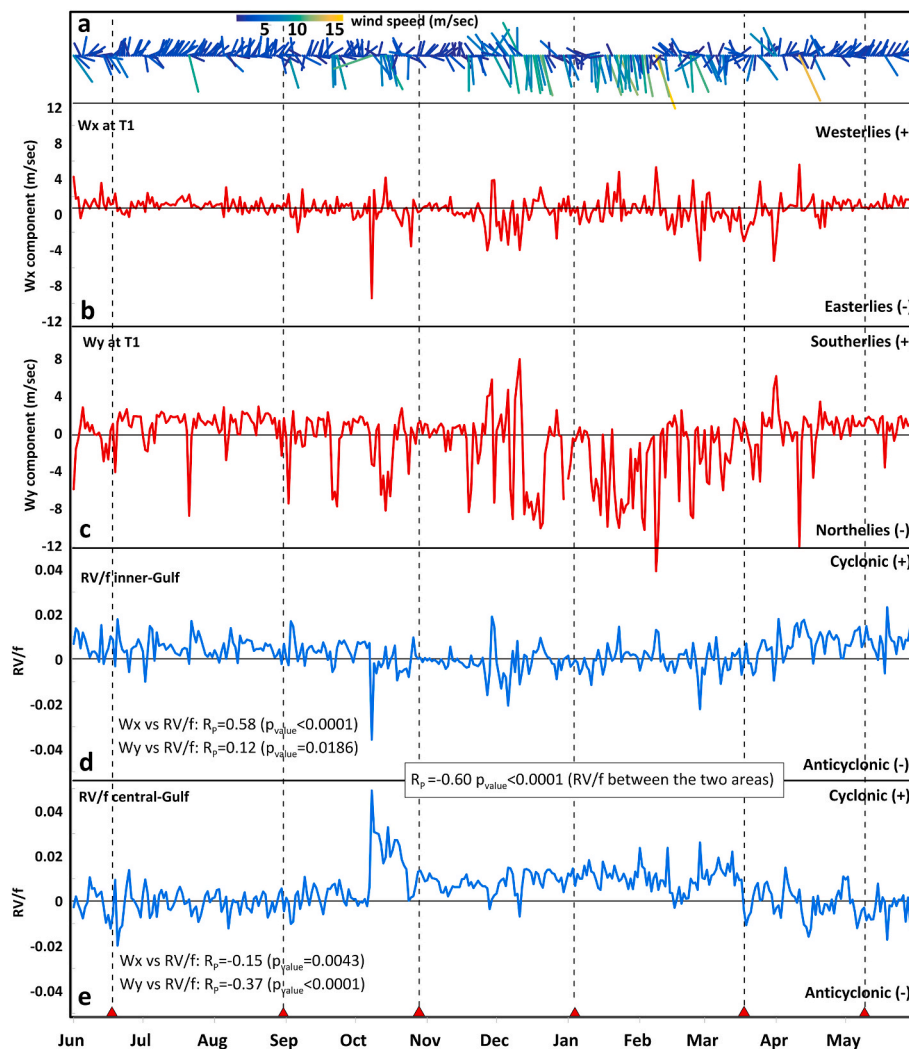


**Fig. 9.** Mean daily timeseries of (a) wind vectors at section T1 (Fig. 1a), (b) zonal component of the wind ( $W_x$ ), (c) meridional component of the wind ( $W_y$ ), ratio of surface Relative Vorticity to Coriolis frequency ( $RV/f$ ) averaged over the (d) inner-, and the (e) central-Gulf during the study annual cycle (1/6/2021–31/05/2022). The Pearson correlation coefficients ( $R_p$ ) and respective MK statistical significance tests ( $p_{value}$ ) are shown. The 6 vertical dashed lines represent the dates of the field campaigns (Table 1).

The zonal component of the wind ( $W_x$ ; Fig. 9b) showed a strong correlation with RV/f of the inner-Gulf (Fig. 9d), confirming the similar variability of the two parameters; the Pearson correlation coefficient is positive, relatively high ( $R_p = 0.58$ ) and statistically significant ( $p_{value} < 0.0001$ ), based on the Mann-Kendall (MK) correlation test (Mann, 1945; Kendall, 1975; i.e., at least 1% significance or 99% confidence levels). Easterly winds (negative  $W_x$ ; Fig. 9b) coincided with negative RV/f values (anticyclonic vorticity; Fig. 9d), while westerly winds (positive  $W_x$ ) enhanced the formation of cyclonic circulation (positive RV/f) in the inner-Gulf. The large negative and positive RV/f peaks occurred when  $W_x$  showed high negative and positive values, respectively. In the central-Gulf (Fig. 9e), the relation between the zonal wind component and vorticity was reversed and weaker (e.g. easterly winds enhanced the cyclonic circulation). The respective Pearson coefficient is lower ( $R_p = -0.15$ ) and although the correlation is also statistically significant, the  $p_{value}$  is larger than the one derived for the inner-Gulf ( $p_{value} = 0.0043$ ), expressing very weak influence of the zonal wind component on the circulation of the central-Gulf. Note that positive and negative values of correlation coefficients represent the relation of the same and the opposite wind and vorticity signs, respectively, as presented in Fig. 9.

The meridional component of the wind ( $W_y$ ; Fig. 9c) revealed positive correlation with RV/f in the inner-Gulf (Fig. 9d) and negative correlation (counter-correlation) with RV/f in the central-Gulf (Fig. 9e). The respective Pearson correlation coefficient is relatively high, negative ( $R_p = -0.37$ ; higher counter-correlation), and statistically

significant ( $p_{value} < 0.0001$ ) for the central-Gulf. The dominance of southerly winds (positive  $W_y$ ) enhanced the formation of anticyclonic circulation over the central-Gulf (negative RV/f), in agreement with the field experiments presented in Section 3.1. On the contrary, northerly winds (negative  $W_y$ ) prevailed mainly between October to March (Fig. 9c) when the RV/f was mainly positive attributed to the cyclonic circulation over the central-Gulf. In the inner-Gulf, the correlation between the meridional wind component and vorticity was positive (northerlies coincide with anticyclonic and southerlies with cyclonic circulation), but it is weaker ( $R_p = 0.12$ ; Fig. 9d) and not statistically significant ( $p_{value} = 0.0186 > 0.01$ ). The two wind-ocean combinations show that the zonal wind component is more related to the near-surface circulation patterns of the inner-Gulf ( $R_p = 0.58$ ), while the meridional component is more important for the central-Gulf ( $R_p = -0.37$ ).

The major but opposite circulation patterns presented above are also confirmed by the RV/f correlation between the inner- and central-Gulf (Fig. 9d and e); the RV/f sign between the two sub-basins is usually opposite, resulting to statistically significant negative Pearson coefficient ( $R_p = -0.60$ ;  $p_{values} < 0.0001$ ). Negative RV/f levels of the inner-Gulf usually coincide with positive central-Gulf values and vice versa (Fig. 9d and e). The respective cross-correlations in the inner- (Fig. 10e) and central-Gulf (Fig. 10f), showed that the highest coefficients occurred at zero lag days, confirming the direct response of circulation on wind conditions. Maps of near-surface RV/f averaged over all periods of the study annual cycle that are characterized by the four wind components (northerlies, southerlies, easterlies, westerlies) with magnitudes over 5

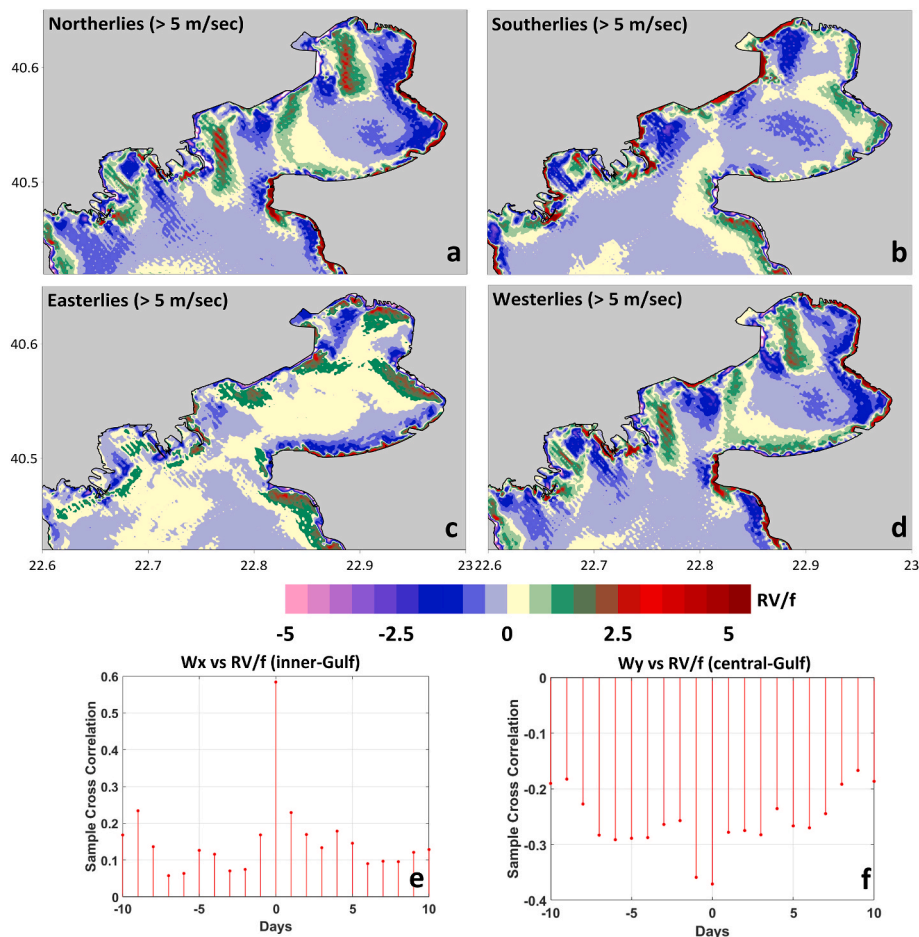


Fig. 10. Maps of Relative Vorticity over Coriolis frequency (RV/f), averaged over the study year's periods with (a) northerly (b) southerly, (c) easterly, and (d) westerly wind component with magnitude higher than 5 m/s, derived from the 3-hourly simulated near-surface currents. The cross correlation and the respective lag (days) between (e) the zonal wind component ( $W_x$ ) and the RV/f, averaged over the inner-Gulf, and (f) the meridional wind component ( $W_y$ ) and the RV/f, averaged over the central-Gulf.

m/s, are presented in Fig. 10. High negative RV/f values were computed over the eastern inner-Gulf and high positive RV/f over the western part of the basin (Fig. 10a) when the southward wind component (northerlies) was strong (>5 m/s). A similar RV/f distribution was derived for the periods with strong westerly components (Fig. 10d). Note that the prevailing winds directions during the study annual cycle, presented in Fig. 2b, show that the northerly and westerly components usually coincide, expressing that the dominant direction is from the northwest (northwesterlies, i.e., Vardar wind, a well-known local ravine aeolian pattern). The southward jet along the western part of the inner-Gulf (cyclonic circulation) highlights the connectivity pathway between the inner- and central-Gulf described by Drifter D7 (Fig. 7). The simultaneous existence of these two counter-rotated patterns in the western (cyclonic) and eastern (anticyclonic) parts of the inner-Gulf explain its general low spatially mean values (Fig. 9d) in comparison to the central-Gulf (Fig. 9e).

The southerly winds affect the eastern part of the inner-Gulf, increasing the RV/f to positive values representing the formation of cyclonic pattern around the coast (Fig. 10b). Contrary to the westerly winds, the strong easterly winds that usually coincide with southerly winds (Fig. 2b) enhance the formation of anticyclonic (northward pathway) along the western coasts of the inner-Gulf (Fig. 10c). In the central-Gulf, a clear cyclonic pathway connected the western and

eastern coasts under strong northerly winds (Fig. 10b). The western part of the central-Gulf (22.85°E) revealed positive (cyclonic) signs of the RV/f under both northerly (Fig. 10b) and westerly (Fig. 10e) winds. Under southerly winds the anticyclonic circulation is evident over the entire central-Gulf (Fig. 10c). On the contrary, the easterly wind component has negligible impact on the central-Gulf circulation (Fig. 10d).

### 3.3. Renewal of the northern Thermaikos gulf

The exchange of water masses across sections T1 and T2, located at the entrances of the inner- and central-Gulf, respectively, control the renewal of the two enclosed sub-basins (Androulidakis et al., 2021). Herein, we investigate the exchanges across the two sections over the entire water column during the study’s annual cycle (2021–2022), based on the vertical distributions of 3-hourly horizontal currents from the Delft3D-Thermaikos numerical simulations (Fig. 11).

During strong northerly winds (e.g., negative  $W_y$  values in mid-July, early-September, mid-September; Fig. 11a), the two-layer flow across the eastern section T1 (location T1E) was typically more intense, with southward flows over the upper 15 m and especially high magnitudes (<-0.2 m/s) in the upper 5 m. Northward flows (>0.15 m/s) mainly observed in the deeper 15–20 m (Fig. 11b). The near-surface southward

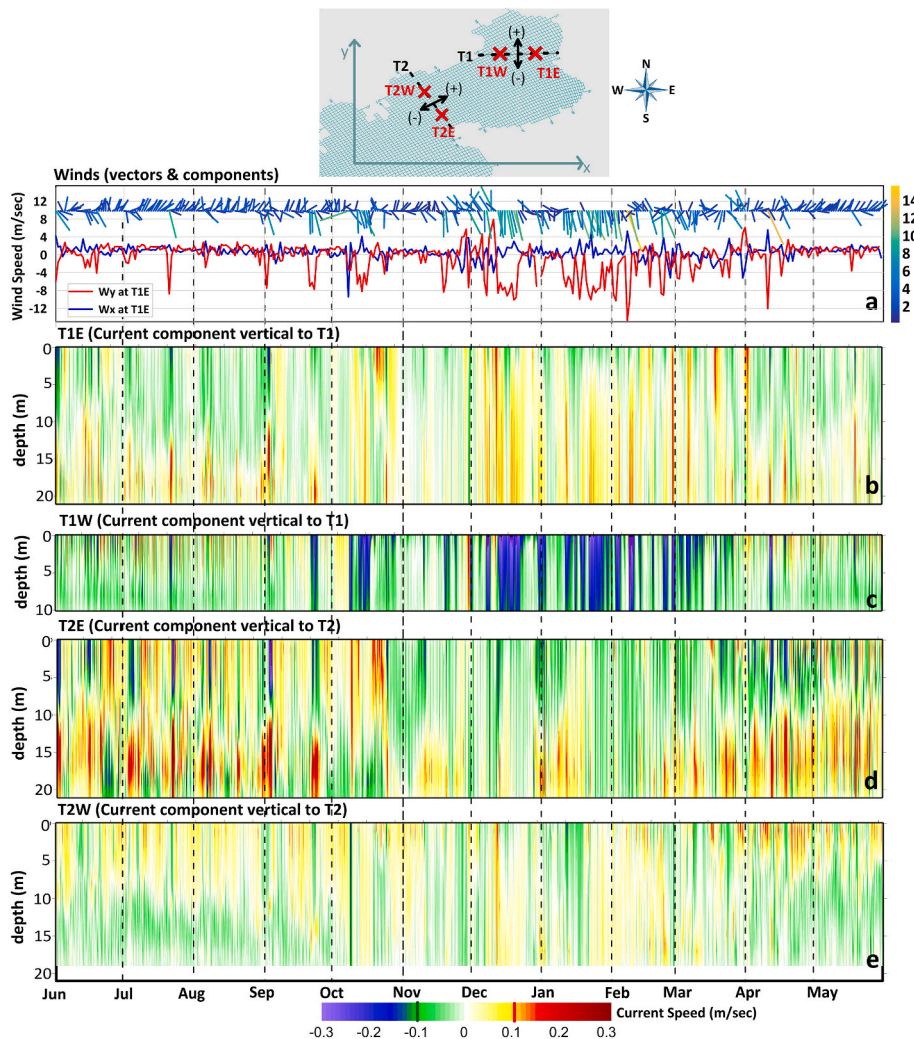


Fig. 11. Timeseries of (a) mean daily meridional ( $W_y$ ; red line) and zonal ( $W_x$ ; blue line) wind components at T1E overlaid by the wind vectors, 3-hourly vertical distributions of the current component vertical to section T1 at locations (b) T1E (east) and (c) T1W (west), and 3-hourly vertical distributions of the current component vertical to section T2 at locations (d) T2E (east) and (e) T2W (west). The contours of the 0.1 and  $-0.1$  m/s velocities are highlighted with orange and green thick lines, respectively. The locations and flows’ directions (velocity signs) are marked in the map (positive inflow, negative outflow).

flow is associated with the anticyclonic circulation that extends along the eastern coasts of the inner-Gulf under northerly winds (Fig. 10a). The deep northward currents along the eastern coasts allow the inflow of waters into the inner-Gulf. On the contrary, the flow over the shallower western part of section T1 (location T1W; 10 m) was southward (negative velocities:  $<-0.2$  m/s), evident along the entire water column during the same periods (northerlies), enhancing the outflow of inner-Gulf water masses along the western coasts towards the central-Gulf (Fig. 11c). It is shown that northerly winds enhance the removal of the surface water masses over the entire water column along the shallower western coasts due to a direct southward jet in agreement with the pathway of Drifter D7 (Fig. 7). The inflow of clearer waters is allowed only along the eastern deeper layers (below the surface outflow).

A two-layer flow was also apparent at location T2E of section T2 (Fig. 11d). The cyclonic (along the eastern coasts) inflow of open sea waters in the deeper layers ( $\sim 0.3$  m/s) was also evident at location T2E (entrance of central-Gulf) during periods with northerlies. This result agrees with previous findings by Krestenitis et al. (2012) who suggested that a clear cyclonic pathway of open sea waters evolves in the near-bottom layers when northerly winds prevail, supporting the overall renewal of the NTG. The northward deep currents were part of the cyclonic circulation around the gulf, supporting the inflow of ASWs. The ASWs in the deeper layers may strengthen the water column stratification between the two water masses (of the Aegean and NTG) in all stations (e.g., at 20 m depth towards the end of August; Fig. 3b). In the near-surface layers, a southward flow of waters is observed in the upper 10 m, removing central-Gulf waters towards the outer-Gulf. The flow exchanges across the western part of section T2 (location T2W) were characterized by weaker current velocities over the entire water column (Fig. 11e).

During periods with southerly winds, the current vertical profile at the eastern part of the inner-Gulf entrance (T1E) is characterized by a reversed two-layer flow with usually positive (northward) currents near the surface (Fig. 11b), associated to the cyclonic circulation in the inner-Gulf (Fig. 10b). Over the western part, the current speeds are very small over the entire water column, showing weak northward flows (positive values) in the upper layers (Fig. 11c). The northward flow along the western coasts was detected at the end of August (Stations SIW, SCW, SON; Fig. 5b) leading to chl-a increases (Fig. 2d) under southerly winds (see Section 3.1). Southerly winds also influence the flows across the

eastern part of section T2 (T2E; Fig. 11d), inducing northward flows towards the central-Gulf, especially over the upper 10 m. This feature was apparent from June to October and from April to June (Fig. 11d), during the periods of prevailing southerly winds (Fig. 11a). Weaker but also northward flows were detected over the western part of the central-Gulf entrance (T2W; Fig. 11e) during the same periods confirming that southerly winds enhance the transport of near-surface waters into the areas north of the Cape Megalo Emvolo (central- and inner-Gulf).

The net transport across section T1, computed at the entire water column ( $Q_{\text{Net}} = Q_{\text{inflow}} + Q_{\text{outflow}}$ ), agrees with the direction of the meridional component of the wind showing strong positive (northward) transport under southerly winds and negative sign (southward) under northerly winds (Fig. 12a). The dominance of the northerly winds enhances the removal of waters over the entire water column at the west of the entrance (T1) and over the upper layers at the east, controlling the negative  $Q_{\text{Net}}$  values across the entrance. The correlation between wind and transport is positive and high ( $R_p > 0.50$ ), while the strongest correlation was computed (not shown) for zero lag days, confirming the direct response of transport across T1 to wind variability.  $Q_{\text{net}}$  across the entrance of the central-Gulf also coincided with the wind variability ( $R_p = 0.30$ ; Fig. 12b), showing strong outflow (negative-southward values indicate flows towards the outer-Gulf) during northerly winds (negative  $W_y$ ), supporting the renewal of the northern sub-basins. The southward direction of the net transport mainly consisted of outflows (southward flows) over the upper layers, allowing the inflows (northward flows) of deeper and denser waters along the eastern coasts. During these periods, the renewal time of the inner-Gulf, which is computed based on the ratio between the inner-Gulf volume ( $V$ ) and the  $Q_{\text{inflow}}$  across section T1 ( $V/Q_{\text{inflow}}$ ) is minimal ( $<2$  days; Fig. 12c) supporting the faster renewal of the northernmost sub-basin of NTG. It is noted that the renewal of the inner-Gulf, discussed here, does not necessarily reflect to the complete cleaning of the basin, since the new-coming waters cannot always be considered “as clean as open sea waters”. However, the renewal processes that replace inner-Gulf water masses with waters originated from the southern basins (central- and outer-Gulf), can be beneficial for its quality since these southern water masses are usually clearer than the water masses in the confined northern part (Krestenitis et al., 2023). The lowest renewal rates were computed in mid-December when continuous northerly winds occurred (Fig. 12a). On the contrary, the longest renewal durations ( $>12$  days; Fig. 12c) occurred when winds were weak

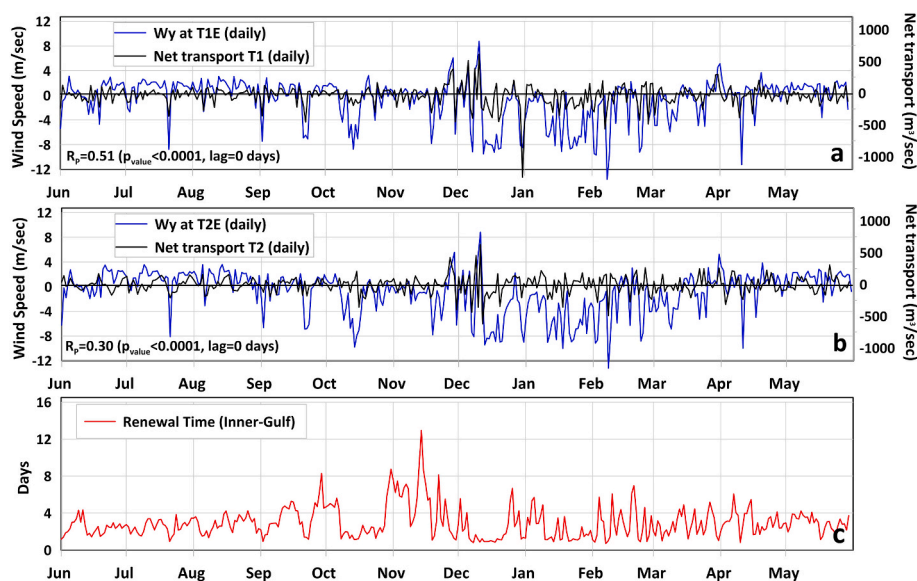


Fig. 12. Timeseries of mean daily meridional ( $W_y$ ; m/sec) and net transport ( $\text{m}^3/\text{sec}$ ) in the entire water column (a) at location T1E and across section T1, and (b) at location T2E and across section T2, respectively from June 2021 to May 2022. The correlation coefficients ( $R_p$ ), the respective MK correlation tests ( $p_{\text{value}}$ ), and the lag (days) between the two timeseries for each section are also presented. (c) Renewal time (days) of the inner-Gulf (north of section T1).

(e.g., 25 October to 20 November; Fig. 12a). Southerly winds mainly induce positive net transport (Fig. 12b) that takes place over both the east (Fig. 11d) and west (Fig. 11e) parts of the central-Gulf entrance.

## 4. Discussion

### 4.1. Interannual variability of physical properties

The variability of the NTG physical properties, measured during the June 2021–May 2022 period, is compared to the respective distribution derived from successive measurement campaigns between 1997 and 2007 (Fig. 13). The setup and main findings of these field studies were presented by Krestenitis et al. (2012). The temperature and salinity profiles at the same six locations were used to derive the evolution of the thermohaline properties, averaged at five layers: i) All Depth (H), ii) Surface Layer (SL: 0–5 m), iii) Upper Intermediate Layer (UIL: 5–10 m), iv) Lower Intermediate Layer (LIL: 10–15 m), and v) Bottom Layer (BL: >15 m). The same approach and annotations with Krestenitis et al. (2012) were used for consistency and comparison reasons. Note that Krestenitis et al. (2012) have derived the mean values from all available stations (>24) for a longer period (1993–2007); for consistency, only the six same stations (out of the 24) were used herein to compare them with the measurements performed in this study.

The SL temperature revealed the highest values in the summer of 2007 (Fig. 13a) associated with an extreme MHW event that occurred in the Aegean Sea (Mavroukis and Tsiros, 2019). Similar MHW events increased the SL temperature (>28 °C; Fig. 3b) in the summer of 2021

(during July and August) almost over the entire water column in all stations (Androulidakis and Krestenitis, 2022). The extremely warm conditions of 2021 also affected the deeper layers of NTG, which showed the highest mean BL temperature (marginally >27 °C) compared to the previous observational periods (<26 °C; Fig. 13a). The intermediate layers were even warmer and closer to the SL levels. The “All Depth” averaged values during August 2021 were the highest among all years (27.6 °C). The MHWs of August 2021 were associated with the air temperature maxima (Fig. 2a; <https://www.noaa.gov/news/august-2021-was-earths-sixth-warmest-august-on-record> accessed on 03 June 2022). The effect was apparent over the upper 15 m of the water column, where all measured temperature values were higher than 27 °C in all regions (Fig. 3b) with salinity levels lower than 37, resulting in rather low densities and weak stratification in the upper water column (<1024 kg/m<sup>3</sup>; Fig. 3b). The temperature minima during the 2021–2022 annual cycle were also relatively higher (~11 °C; March 2022) in comparison with temperatures derived from most of the previous available measurements, ranging around the levels of the 1997–1998 observational period (Fig. 13a). This is in agreement with Androulidakis and Krestenitis (2022), who, based on long-term satellite observations, showed that besides the increasing summer temperatures a significant interannual positive trend is also apparent during the cold months of the year (winter-spring)

A more profound difference between the recent year (2021–2022) and the 1997–2007 period was detected for the salinity interannual variability (Fig. 13b). The “All Depth” averaged values were higher during the 2021–2022 period for all seasonal campaigns, except from

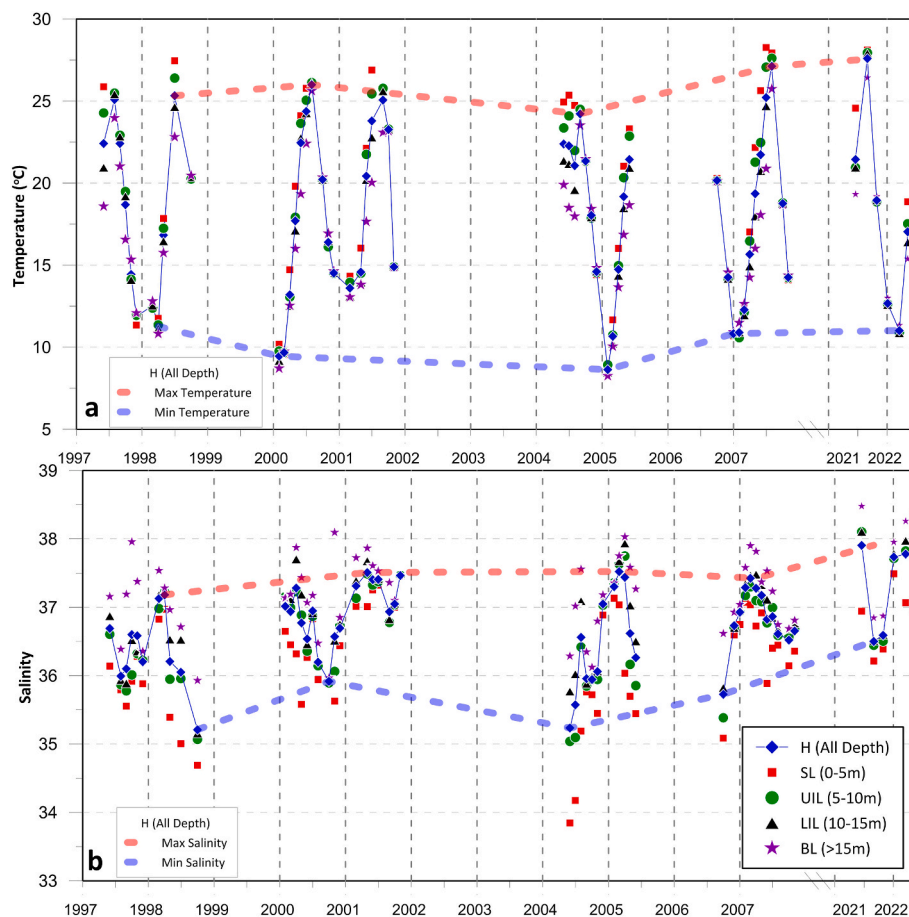


**Fig. 13.** Temporal evolution of (a) temperature and (b) salinity derived from the 6 study stations for four observational periods from 1997 to 2007 (Krestenitis et al., 2012) and one observational period from 2021 to 2022. The plotted values include the entire water column (H, noted with solid blue line), the Surface Layer: SL, the Upper Intermediate Layer: UIL, the Lower Intermediate Layer: LIL, and the Bottom Layer: BL. The red and blue dashed lines represent the envelope and show the evolution of the maximum and minimum temperature and salinity values for each observational period.

summer, with notably saltier waters during the winter and spring months (Fig. 13b). The recent observations showed that the water masses of the intermediate and near-bottom layers were the saltiest among all years, revealing the highest values in the BL of June 2021, and March and May of 2022. Both maximum and minimum salinity levels of 2021–2022, averaged over the entire water column (“All Depth”), were the highest in comparison to the values derived from all observational periods, ranging around 38 and 36.5, respectively. The increased salinity levels during the recent year might be mainly attributed to three reasons: i) reduction of the river discharge rates (mean annual discharge of Axios derived from the 2017–2021 period, using the same measurements presented in Fig. 2c, was around  $70 \text{ m}^3/\text{s}$ , while Antonopoulos and Tsiouris (1991) and Van Gils and Argiropoulos (1991) reported a mean annual river discharge of  $135 \text{ m}^3/\text{s}$  and  $150 \text{ m}^3/\text{s}$ , respectively); ii) possible interannual changes on evaporation-precipitation rates; and iii) possible interannual changes of the wind state that may have altered the renewal and hydrodynamic circulation of the NTG, enhancing the inflow of saltier waters into the Gulf. To confirm the above hypotheses, an interannual meteorological and land-river drainage focused analysis is required, which was though out of our study’s scope.

#### 4.2. General circulation patterns

A schematic of the general circulation of the NTG as gleaned from the field observations and the numerical simulations is presented in Fig. 14. We discuss the circulation features that usually form during the dominant (meridional components stronger than zonal components) northerly and southerly wind components, which however typically coincide with the weaker westerly and easterly components, respectively (insert in Fig. 14; northwesterlies and southeasterlies). Krestenitis et al. (2012), based on geostrophic currents derived from long-term thermohaline observations, showed that the hydrodynamic horizontal circulation generally takes place in two layers with a strong seasonal variability. The prevailing circulation and its relation to the wind directions at each sub-basin is largely influenced by the coastline morphology of the NTG.

Under northerly winds, the waters of the inner-Gulf may propagate cyclonically either along the western coasts towards the outer-Gulf or directly southward reaching the broader central-Gulf (Fig. 14a). The latter pathway is very crucial for the seawater quality of the central-Gulf because, although it contributes on the renewal of the inner-Gulf, it

enhances the physical connectivity of the most polluted inner-Gulf surface waters (Thessaloniki city front, port, and industrial area) and coastal areas with tourist activities and infrastructure (e.g., eastern coasts of the central-Gulf). The cyclonic surface circulation takes place mainly in the near-surface layers of the central-Gulf, spreading waters along the eastern coasts in agreement with Krestenitis et al. (2012). A clear southward pathway is also formed over the outer-Gulf connecting the NTG with the western coasts of the southern Thermaikos Gulf. This southward pathway may also supply nutrient-rich waters to the broader northern Aegean Sea via the general cyclonic circulation of the Aegean archipelago basin (Zervakis and Georgopoulos, 2002; Androulidakis and Kourafalou, 2011; Androulidakis et al., 2012).

The southerly winds enhance the formation of anticyclonic eddies at both the outer- and central-Gulf (Fig. 14b). Northward near-surface currents mainly occur over the inner-Gulf but with opposite vorticity signs over its western and eastern parts; a cyclonic flow is formed around its eastern coasts and an anticyclonic branch along the western coasts, increasing the renewal time of this northernmost region, in agreement with Androulidakis et al. (2021). The northward and onshore currents in the vicinity of the deltas, together with the anticyclonic patterns, may spread the low salinity waters along the entire western coast of the NTG. The anticyclonic circulation in the outer-Gulf minimises the exchanges between the central and outer basins and the renewal of the northern water masses.

Five types of flow are more dominant across the two entrances (Fig. 14): 1) a more common two-layer transport along the eastern coasts, with southward outflow towards the central-Gulf in the upper layer ( $<15 \text{ m}$ ) and northward inflow towards the inner-Gulf in the deeper layer ( $>15 \text{ m}$ ) under northerlies; 2) a reversed two-layer transport at the same area under southerly winds; 3) a southward flow along the western coasts and the entire water column of the inner-Gulf that connects the inner-Gulf with the central-Gulf under northerlies; 4) a two-layer flow over the eastern part of the central-Gulf entrance (southward flow in the upper layers and northward flows in the deeper layers) under northerlies; and 5) a northward flow over the upper-layers ( $>10 \text{ m}$ ) across the entrance of the central-Gulf under southerly winds.

#### 4.3. Limitations of the observational approach

The main limitation of the study is related to the restricted ability for

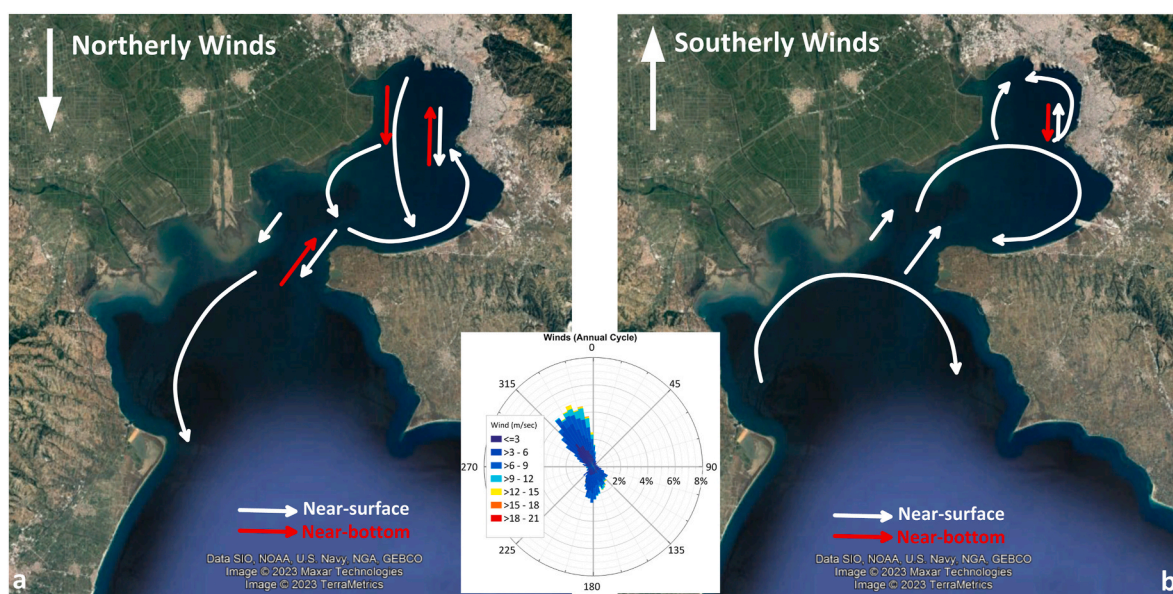


Fig. 14. Schematic representations of general circulation features of NTG under (a) northerly and (b) southerly winds. The white and red solid lines present the near-surface and near-bottom circulation patterns, respectively. The insert rose diagram presents the 3-hourly wind vectors, averaged over the NTG, for the entire study year (June 2021–May 2022; the direction represents the origin of the wind).

seasonal interpretation of our findings due to the infrequent nature of the six (bimonthly) campaigns. Moreover, although the locations of the measurements were selected in such a way to cover all the major sub-basins of the gulf, more stations between the current ones would provide more information about the in-between water masses. These discrepancies were tackled with the support of numerical simulations and satellite data that provided continuous information over the entire study region during the study year. Another limitation is related to the “big unknown” of the gulf, namely the river outflows. Although their discharge rates are relatively small, the brackish plume, especially from the large Axios and Aliakmonas rivers, may affect the stratification of the water column and furthermore the hydrography and quality of the water masses of the semi-enclosed basin of NTG. To overcome this uncertainty, we have developed hydrological simulations that were combined with available river discharge rate measurements to provide updated annual timeseries of daily outflow rates for several freshwater sources, useful for further interdisciplinary studies. A third limitation is associated with the representativeness of the measurement stations for each sub-basin in comparison to previous observational studies (Kresitenis et al., 2012) that included a larger number of stations. For consistency, only the exact same stations from older campaigns (e.g., 1997–2007) were compared with the most recent ones (2021–2022) to evaluate the interannual variability and detect potential differences. Moreover, we showed that the current measurements at the six stations agree with the circulation patterns derived from both drifter trajectories and simulated currents that cover the entire NTG domain. Finally, the use of chl-a concentrations to identify river plume spreading everywhere in the Gulf (especially away from the river mouths) was avoided. Although brackish waters can be associated with the chl-a peaks due to nutrient abundance, they do not constitute the only factor responsible for the high primary productivity. Other physical and biochemical processes, which are out of the scope of this study, are also involved in shaping the primary productivity of the water column.

#### 4.4. Future steps and recommendations

Our observational findings highlighted the crucial need for continuous, spatially and temporally denser monitoring of this environmentally vulnerable coastal basin, whose seawater quality is influenced by several anthropogenic pressures (numerous point and diffuse pollution sources such as the agricultural drainage outflows) and natural factors (river discharges, met-ocean conditions, coastal waters' exchanges with the open sea, etc.). Our results showed that continuous monitoring (e.g., with permanent monitoring buoys) over the entire water column at the two entrances (Cape Mikro Emvolo and Cape Megalo Emvolo) would provide vital real-time information about the renewal ability of the enclosed basins. Moreover, monitoring the near-surface circulation over the entire inner- and central-Gulf with the use of High Frequency Radars, which are broadly used in application at semi-enclosed basins (i.e., Falco et al., 2016; Tran et al., 2022) would also be a very useful operational tool for the holistic understanding of the NTG.

A crucial future step is to upgrade the existing operational modeling platform (Wave4us; <http://wave4us.web.auth.gr>), used in the current study, by adding the component of the biogeochemical processes (biogeochemical modelling) to predict and analyse the relevant processes and potential eutrophication events over the ecologically sensitive environment of Thermaikos Gulf. Such integrated operational systems that include the input from pollution sources in detail (e.g., freshwater sources) would be extremely beneficial for NTG stakeholders (e.g., touristic, athletic, fisheries and aquaculture activities) and authorities (e.g., first-responders, coastal/urban managers etc.). It is noted that the development of these systems requires real-time estimation of the pollution input (e.g., chemical characteristics, discharge rates), which is unfortunately missing for now at the numerous freshwater sources along the NTG coastline.

Severe meteorological events that usually occur during the summer

and autumn months (e.g., Medicanes; Nastos et al., 2018) over the central Mediterranean and became stronger during the last decades may affect the coastal areas of Thermaikos Gulf with strong storm surges (Androulidakis et al., 2023) and extremely high precipitation rates, extensive flooding followed by very strong outflows with polluted waters into the marine environment. For example, the most recent storm that affected the region southwest of Thermaikos (Storm Daniel) on 4–8 September 2023 ([https://www.meteo.gr/article\\_view.cfm?entryID=2915](https://www.meteo.gr/article_view.cfm?entryID=2915); last accessed on 17/09/2023) was characterized by precipitation rates over 500 mm/24h that caused extensive flooding, destructions of infrastructure, losses of life and finally significantly strong discharge of polluted freshwaters into the southern Thermaikos Gulf through the Pineios Delta (Fig. 15a). The direct increase of chl-a concentrations, as derived by satellite ocean color multi-sensors (Copernicus Marine Service; <https://marine.copernicus.eu/>; last accessed on 17/09/2023) over the southern gulf (Fig. 15b) is a clear indication that these polluted waters might quickly affect several areas of interest (touristic, fisheries, coastal cities etc) over the entire Thermaikos Gulf, depending on the prevailing ocean circulation conditions. To address this type of events, especially in the context of climate change that may increase their intensity and frequency, it is required to (a) operate and produce regional fast predictions with real-time forecasts, integrating atmospheric, drainage, river and marine conditions and (b) design a well-prepared monitoring platform, ready to be in place quickly to collect measurements over the affected marine areas of Thermaikos Gulf.

## 5. Conclusions

A multi-platform observational and modeling study was conducted to describe the hydrography and the main circulation patterns of the Northern Thermaikos Gulf (NTG). It is the first time that drifter trajectories were used to describe the physical connectivity in NTG, representing the near-surface circulation pathways under variable wind regimes. The response of the ocean circulation patterns to wind variability is direct and does not show any time lag. It is shown that the wind variations control: i) the vorticity signs of the circulation patterns in the three sub-basins of NTG (inner-, central-, and outer-Gulf), ii) the exchanges in the upper and deeper layers between the sub-basins and the renewal of the enclosed areas, and iii) the spreading of riverine waters over the NTG. It is shown that the wind-induced circulation plays a more determining role on the hydrography of the semi-enclosed basin than the variability of the river discharge rates, especially over the most distant areas from the river deltas (e.g., eastern central-Gulf and inner-Gulf). The southward removal of surface waters and the inflow of clearer Aegean Sea Waters (ASW) in the deeper layers determine the efficient renewal and quality levels of the NTG water masses.

The field observations (drifter trajectories and current measurements) *in tandem* with simulated results showed that the northerly winds may minimise the inflow of surface waters into the northern part of NTG but enhance the cyclonic circulation along the eastern coasts. Moreover, the northerly winds contribute to the southward removal of surface brackish nutrient-rich waters, increase the salinity levels by allowing the inflow of deeper, denser water masses, and may form conditions unfavourable to eutrophication, especially at the northern basins of the gulf (Androulidakis et al., 2021). A direct connectivity pathway between the northern coast of the gulf and the eastern coasts of the central-Gulf is formed along the western coasts of the inner-Gulf when strong northerly winds prevail. This circulation pathway, that is apparent in the entire water column, may remove polluted waters from the northern part (e.g., pollutants from port operations, industrial area's effluents, oil spills, release of untreated wastewater; Androulidakis et al., 2021) affecting the water masses along the southeastern coastal areas of the central-Gulf, which are characterized by extensive touristic activities (22.8–22.95°E and 40.5°N). These coastal areas can be impacted by polluted waters, without having themselves sources of strong

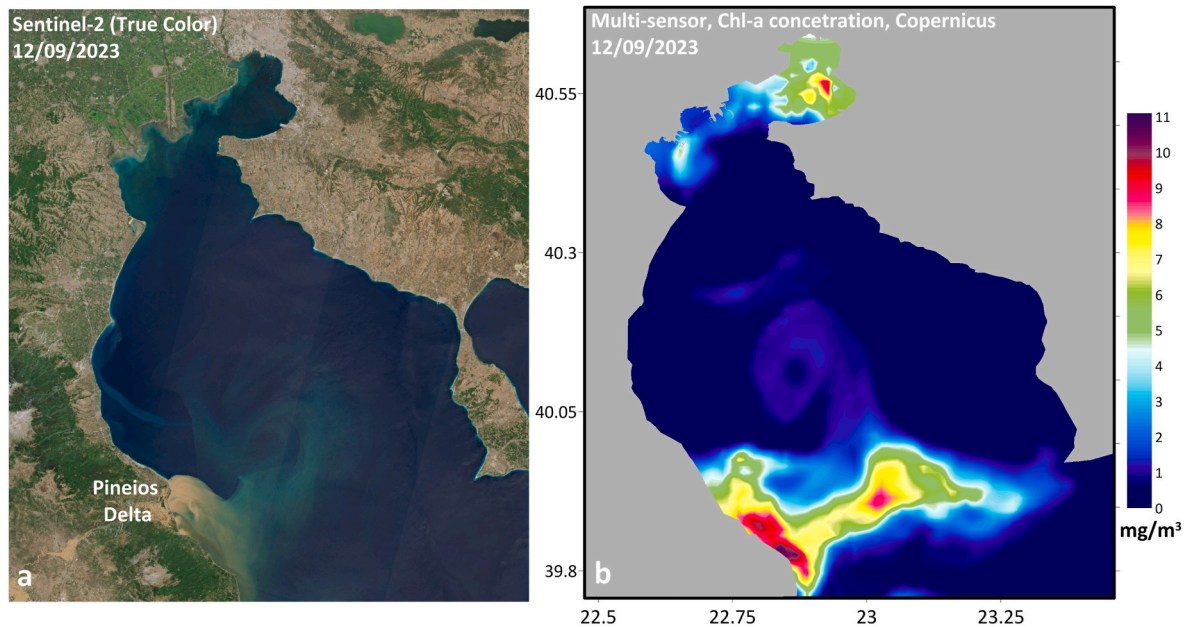


**Fig. 15.** Expansion of the Pineios river plume over the southern Thermaikos Gulf as derived by (a) the Sentinel-2 true color image and (b) the chl-a concentrations of the Copernicus multi-sensor satellite product on 12/09/2023.

environmental stresses (origins of pollution). An anticyclonic circulation prevails in the surface of the eastern inner-Gulf, where together with the inflow of deeper waters along the eastern coasts, establish a two-layer flow at the eastern part of the entrance in the vicinity of Cape Mikro Emvolo (Fig. 1a). A cyclonic circulation pattern prevails at the surface of the broader central-Gulf. A two-layer flow is also detected at the entrance of Cape Megalo Emvolo (Fig. 1a) allowing the inflow of ASW from the outer-Gulf into the northern sub-basins that may contribute on the renewal of the NTG. Under northerly winds, the surface water masses of the outer-Gulf are removed southward, spreading the low-salinity waters along the western coasts of the broader Thermaikos Gulf reducing the renewal time of the northernmost enclosed basin (<2 days).

The two anticyclonic patterns that form in the outer- and central-Gulf, under southerly winds, weaken the exchanges between the three sub-basins of the gulf and especially minimise the southward removal of the surface waters. The anticyclonic eddy over the outer-Gulf may also spread the brackish waters from the deltas offshore before their entrainment into the general cyclonic circulation around the northern Aegean Sea coasts (Zervakis and Georgopoulos, 2002; Androulidakis and Kourafalou, 2011; Androulidakis et al., 2012). Southerly winds may also drag the riverine waters towards the shore and spread them along the entire west coast, contributing to the eutrophication peaks of the central- and inner-Gulf in agreement with Androulidakis et al. (2021). A cyclonic gyre along the coasts of the inner-Gulf (Thessaloniki Bay) may spread surface waters along the seafront of the city weakening the renewal of the rather confined parts of the bay. The drifter experiments, backed up by *in situ* measurements in coastal waters, reveal that the inner parts of NTG pertain occasional hydrodynamically confined areas. There, closed flow loops are formed at times under a variety of meteorological conditions (except from northerlies) that may undermine the seawater quality of the inner-NTG by confining nutrient-rich or polluted waters in the coastal zone. The semi-enclosed geographical setting of the inner-NTG (Thessaloniki Bay) enhances the possible eutrophication-prone physical (met-ocean) conditions.

The observed temperature levels showed a weak interannual variability; however, the Marine Heat Waves (MHWs) of summer 2021 (Androulidakis and Krestenitis, 2022) affected almost the entire water column leading to the highest temperature values in the upper 20 m of

the entire NTG. The salinity levels of the 2021–2022 period were higher than the recorded ones during the previous years. Namely, a systematic prevalence of higher salinity in coastal sites, detected in our analysis, indicates probable river flow shortage. Potential future changes in the occurrence frequency of the prevailing wind directions may affect the variability of the thermohaline properties, circulation conditions, and connectivity pathways of the NTG. The increase and/or intensification of northerlies may enhance the renewal of the inner parts, the salinity boost, and the southward removal of polluted and nutrient-rich waters. On the contrary, a respective change of the southerly winds can impose weak renewal conditions and confine riverine waters in the northern enclosed basins. Therefore, the importance of a systematic continuous monitoring effort together with an integrated (inland-coastal-ocean waters) operational forecasting system in the NTG waters is demonstrated.

#### Declaration of competing interest

The authors declare that they have no known competing financial interests or personal relationships that could have appeared to influence the work reported in this paper.

#### Acknowledgments

The field campaigns were conducted under the program "Mapping of pressures and estimation of external and internal loads of nutrients and organic material for the protection and management of the marine waters in Thermaikos Gulf" funded by the Management Unit of Protected Areas of Central Macedonia (MUPACM) of the Natural Environment & Climate Change Agency (NECCA). We thank Alexandros Dimitrakopoulos (Laboratory of Physical and Chemical Oceanography in the Department of Marine Sciences, University of the Aegean) for the design and development of the "AEGEAN" drifters. The "CARTHE" drifters were kindly provided by Guillaume Novelli and Cédric M. Guigand (Rosestiel School of Marine and Atmospheric Science, University of Miami). The drifter communication software was developed and provided by Dr. Alkiviadis Kalampokis (Red Sea Research Center, King Abdullah University of Science and Technology, KAUST). We thank Evangelos Hatzigiannakis and Paschalis Dalampakis from the Soil and Water Resources

Institute (SWRI; Hellenic Agricultural Organization “DEMETER”) for providing the discharge rates of Aliakmonas river that were collected in the framework of the project: “Operation of the National Network for the Monitoring and Recording of the Quantity (rivers) and Quality (rivers and lakes) of Greek Surface Water Resources (MIS 5001336)” (<https://www.swri.gr/index.php/el>; <https://www.lri.swri.gr/index.php/el/>).

Mrs. Gioula Tsiknakou and Mr. Stefanos Sarafidis from Terna – Energy S. A. provided the data about the discharge rates of Axios river (<https://www.terna-energy.com/acivities/hydroelectric-projects/shpp-eleoussa/?country=>). We thank Dr. Katerina Kombiadou for her useful comments and suggestions.

## APPENDIX

### 1. Meteorological simulation

Simulations of regional-scale, high-resolution, atmospheric circulation were conducted with the Weather Research and Forecasting model’s Advanced Research dynamic solver (WRF-ARW-AUTH; Wang et al., 2010). The integrated weather forecast system relies on three nested meteorological simulations with increasing resolution, i.e., over the European continent (grid spacing 15 km × 15 km), the central Mediterranean (including Apennine and Balkan peninsulas, with a grid spacing of 5 km × 5 km), and the Central Macedonia (1.67 km × 1.67 km; Fig. 1b) region that includes the Thermaikos Gulf. The produced 3-hourly atmospheric datasets consist of wind velocities, sea level pressure, air temperature, relative humidity, cloudiness, latent heat, and precipitation fields (Pytharoulis et al., 2015a; 2016). The meteorological model was initialized at 12:00 UTC daily, using the global analysis of the Global Forecasting System of NCEP (National Centers for Environmental Prediction) with a grid spacing of 0.25° × 0.25° (<https://www.emc.ncep.noaa.gov/>). The Sea Surface Temperature (SST) values are based on the daily global dataset of NCEP with a grid spacing of 1/12° × 1/12°. The microphysics, cumulus convection in the two outer domains, radiation, boundary layer, surface layer and soil processes (in 4 layer down to 2 m below land surface) are parameterized through the Ferrier (Rogers et al., 2001), Betts-Miller-Janjić (Janjić, 1994, 2000), RRTMG (rapid radiative transfer model application for global climate models; Iacono et al., 2008), Mellor-Yamada-Janjić (Mellor and Yamada, 1982; Janjić, 2002), Monin-Obukhov (Eta; Janjić, 1994; 1996) schemes and NOAA (NCEP/Oregon State University/Air Force/Hydrologic Research Lab) Unified model (Chen and Dudhia, 2001), respectively. The daily output of the 12–33 forecast hours that is utilized in this study are used to force the hydrodynamic simulations. The modelling system has been validated for large periods and for extreme events (Pytharoulis et al., 2015a, 2015b, 2016).

### 2. Hydrodynamic simulation

The coastal circulation simulations were implemented with the FLOW module of the Delft3D (Delft3D-FLOW) modeling system (<https://oss.deltares.nl/web/delft3d>) in a 3-D sigma-layer configuration covering the broader Thermaikos Gulf (Delft3D-Thermaikos; Androulidakis et al., 2021). The model solves numerically the 3-D non-linear shallow water equations, derived from the Navier-Stokes equations for incompressible free-surface flow. Apart from the horizontal equations of motion, the system of model equations consists of the continuity equation and the transport equations for conservative constituents. Real-world applications’ validation and model description of Delft3D-FLOW can be found in Gerritsen et al. (2008).

The sigma-layers configuration of Delft3D allows model coordinates to follow the bottom morphology and is suitable for Mediterranean coastal regions with shallow and complex topography (Zavattarielli and Mellor, 1995). The time-step of the Delft3D-Thermaikos simulations was equal to 30 s to serve the Courant-Friedrichs-Lewy (CFL) criterion. The computation of the wind drag coefficients was based on the parametrization by Amoroso and DeVries (1980). The turbulent flow conditions were simulated with the *k-epsilon* turbulence model. The boundary conditions, i.e., physical properties in the water column along the open southern boundary of the model, are derived by the Mediterranean Forecasting System model (Clementi et al., 2019; <http://medforecast.bo.ingv.it/>) embedded into Copernicus CMS Mediterranean Sea Physical Reanalysis dataset (Simoncelli et al., 2019). The meteorological forcing consists of 3-hourly fields derived from the WRF-ARW-AUTH model, including wind velocities, sea level pressure, air temperature, relative humidity, cloudiness, and precipitation (see previous Section 1). The river input of Delft3D-Thermaikos was based on either measured (Axios and Aliakmonas) or simulated (Gallikos, Loudias, Halastra and Anthemountas) daily rates. The large Axios and Aliakmonas sources were divided to 8 and 3 model cells, respectively, for better representation of the river deltas. Hydrodynamic simulations of Thermaikos Gulf with the modelling system presented herein cover a 6-year period starting on 1/1/2017, providing 3-hourly output of physical properties for the entire water column (e.g., temperature, salinity, density, currents). Androulidakis et al. (2021) discussed in detail the model setup (e.g., initial, boundary, and forcing conditions; parameterizations and river input) and its performance capabilities. Their comparisons with field observations confirmed the efficiency of Delft3D-Thermaikos; the RMSEs of temperature and salinity were 0.67 °C and 0.29, respectively, with high Pearson correlation coefficients ( $R_p > 0.90$ ; their Fig. 8).

We performed additional comparisons for the 2021–2022 period based on the measured profiles in the six NTG stations; the RMSEs and correlation coefficients for temperature and salinity are 1.43 °C and 0.76, and  $R_p = 0.975$  and 0.514, respectively (Table A1). The relatively high RMSE is related to the mid-depth measurements of the August 2021 campaign, where model and observed values revealed larger differences; the exclusion of these measurements from the computation reduces RMSE to 0.78 °C. Moreover, high Willmott Skill Scores (Ws; Willmott, 1981) were computed ( $W_s = 0.98$  and  $W_s = 0.70$ ) using all measurements, while the Cost Function (CF) index (Allen et al., 2007) is lower than 1 for both variables, confirming the good performance of the model.

**Table A1**

Statistical metrics of the model performance using all temperature and salinity measurements at the 6 stations of NTG during the study period (2021–2022).

| Variable         | Mean Error (Bias) | Mean Absolute Error | RMSE    | Cost Function (CF)                  | Willmott Model Skill (Ws)                      |
|------------------|-------------------|---------------------|---------|-------------------------------------|--|
| Temperature      | −0.08 °C          | 0.87 °C             | 1.43 °C | 0.15                                | 0.98   |
| Salinity         | −0.19             | 0.62                | 0.76    | 0.77                                | 0.70   |
| Validation Scale |                   |                     |         | CF < 1: very good<br>CF = 1–2: good | $W_s = 1$ : perfect agreement (Willmott, 1981) |

(continued on next page)

Table A1 (continued)

| Variable | Mean Error (Bias) | Mean Absolute Error | RMSE | Cost Function (CF)                                     | Willmott Model Skill (Ws) |
|----------|-------------------|---------------------|------|--|---------------------------|
|          |                   |                     |      | CF = 2–5: moderate<br>CF > 5: bad (Allen et al., 2007) |                           |

We have also performed an additional comparison to evaluate the model performance, based on satellite-derived Sea Surface Temperature (SST; the NTG resolution is almost 1 km with a daily temporal step based on the L4 product; <https://www.copernicus.eu/>, last accessed on 01/04/2023). The daily SST anomaly (monthly average subtracted) derived from the model and satellite data, averaged over the model domain (Fig. 1b), is presented in Figure A2. Both negative and positive SST anomalies were efficiently reproduced by Delft3D-Thermaikos revealing high correlation ( $R_p = 0.92$ ) and small RMSE ( $<0.5$  °C).

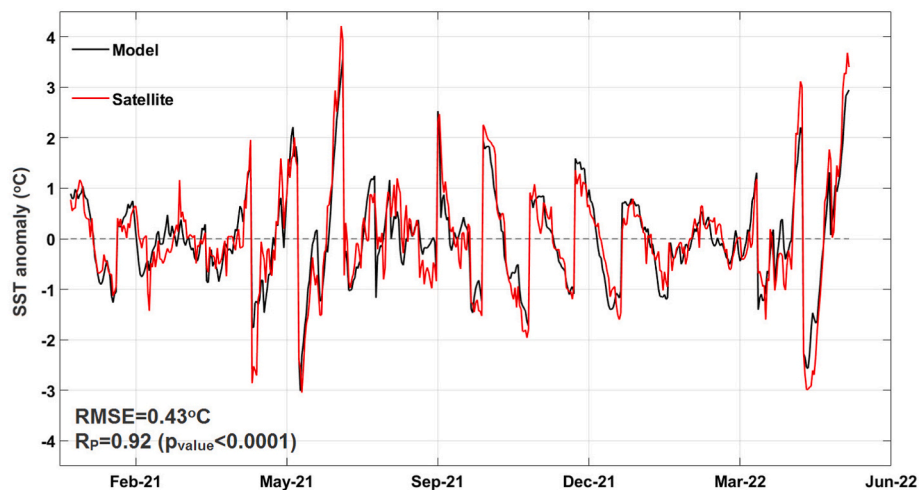
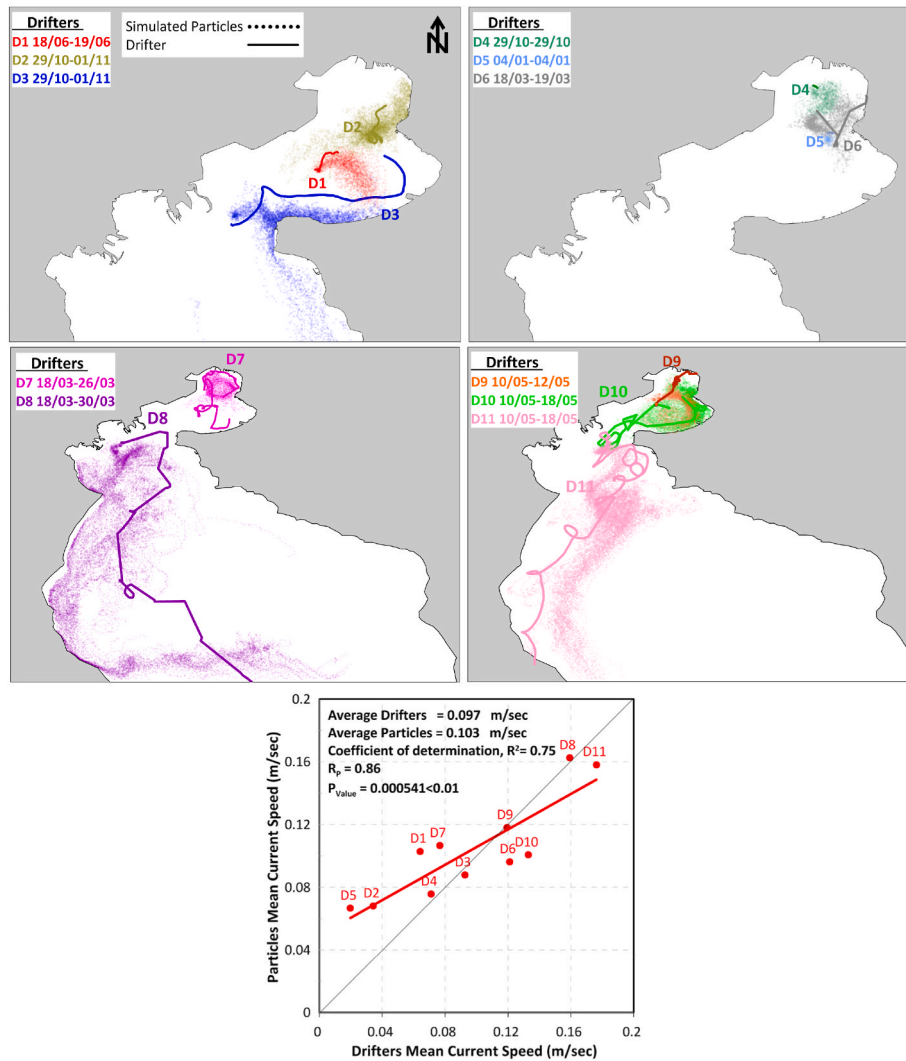


Fig. A1. Comparisons of Sea Surface Temperature anomaly (SST, °C) derived from Delft3D-Thermaikos simulation (black line) and Copernicus satellite data (red line), averaged over the model domain (monthly average subtracted). The Root Mean Square Error (RMSE), the Pearson correlation coefficient ( $R_p$ ), and the respective correlation statistical significance ( $p_{\text{value}}$ ) is shown.

Lagrangian numerical experiments were also developed to evaluate the ability of the model to reproduce the 11 drifter trajectories used in the current study. The Lagrangian simulations were based on the tracer method (random walk method) developed by Krestenitis et al. (2007). Namely, Tracer2Dmodel (<https://repository.kallipos.gr/handle/11419/2786>) simulates the spreading of passive particles, using the surface current fields (layer 1) derived from the Delft3D-Thermaikos simulation. One hundred (100) particles were released at each drifter deployment site and left to circulate for the same periods as the real drifters. The overall trajectories of the 100 particles for each case are presented in Figure A2. In all experiments, the spreading of particles generally agrees with the drifter trajectories, reproducing the prevailing circulation patterns discussed in Figs. 5–8. The regression fit of the current speed derived from field and numerical particles is very close to the “ $x = y$ ” identity line with high  $R_p = 0.86$  and  $R^2 = 0.75$  that are statistically significant ( $p_{\text{value}} < 0.01$ ). The mean current speed derived from all simulated particles ranged around 0.10 m/s and it is very close to the respective drifter mean (Figure A2). The Lagrangian numerical experiments confirmed that the Delft3D-Thermaikos model may efficiently reproduce the drifter trajectories discussed in Section 3.1.



**Fig. A2.** Trajectories of drifters and simulated particles, and statistical comparison (averages, coefficients of determination and correlation,  $p_{value}$ ) of their current speeds.

## References

- Amorcho, J., DeVries, J.J., 1980. A new evaluation of the wind stress coefficient over water surfaces. *J. Geophys. Res.: Oceans* 85 (C1), 433–442.
- Androulidakis, Y., Kolovoyiannis, V., Makris, C., Krestenitis, Y., Baltikas, V., Stefanidou, N., Chatziantoniou, A., Topouzelis, K., Moustaka-Gouni, M., 2021. Effects of ocean circulation on the eutrophication of a Mediterranean gulf with river inlets: the Northern Thermaikos Gulf. *Continental Shelf Res.* 221, 104416.
- Androulidakis, Y., Kourafalou, V., Özgökmen, T., Garcia-Pineda, O., Lund, B., Le Hénaff, M., Hu, C., Haus, B.K., Novelli, G., Guigand, C., Kang, H., 2018. Influence of river-induced fronts on hydrocarbon transport: a multiplatform observational study. *J. Geophys. Res.: Oceans* 123 (5), 3259–3285.
- Androulidakis, Y., Makris, C., Mallios, Z., Pytharoulis, I., Baltikas, V., Krestenitis, Y., 2023. Storm surges and coastal inundation during extreme events in the Mediterranean Sea: the IANOS Medicane. *Nat. Hazards*. <https://doi.org/10.1007/s11069-023-05890-6>.
- Androulidakis, Y.S., Kourafalou, V.H., 2011. Evolution of a buoyant outflow in the presence of complex topography: the Dardanelles plume (North Aegean Sea). *J. Geophys. Res.: Oceans* 116 (C4).
- Androulidakis, Y.S., Krestenitis, Y.N., 2022. Sea surface temperature variability and marine heat waves over the Aegean, Ionian, and Cretan Seas from 2008–2021. *J. Mar. Sci. Eng.* 10 (1), 42.
- Androulidakis, Y.S., Krestenitis, Y.N., Kourafalou, V.H., 2012. Connectivity of North Aegean circulation to the black sea water budget. *Continental Shelf Res.* 48, 8–26.
- Antonopoulos, V., Tsiouris, S., 1991. Relationships between discharges and water quality parameters in the Axios river. In: *Proceedings of the 2<sup>nd</sup> Conference of Environmental Science and Technology, Mitilini, Greece* (in Greek).
- Balopoulos, E.T., Friligos, N.C., 1994. Water circulation and eutrophication in the northwestern Aegean Sea: Thermaikos gulf. *Toxicol. Environ. Chem.* 41 (3–4), 155–167.
- Brockmann, C., Doerffer, R., Peters, M., Kerstin, S., Embacher, S., Ruescas, A., 2016. Evolution of the C2RCC neural network for Sentinel 2 and 3 for the retrieval of ocean colour products in normal and extreme optically complex waters. *ESASP* 740, 54.
- Chen, F., Dudhia, J., 2001. Coupling an advanced land surface–hydrology model with the Penn State–NCAR MM5 modeling system. Part I: model implementation and sensitivity. *Mon. Weather Rev.* 129 (4), 569–585.
- Clementi, E., Pistoia, J., Escudier, R., Delrosso, D., Drudi, M., Grandi, A., Lecci, R., Creti, S., Ciliberti, S.A., Coppini, G., Masina, S., Pinardi, N., 2019. Mediterranean Sea analysis and forecast (CMEMS MED-Currents, EAS5 system) [Dataset]. In: *Copernicus Monitoring Environment Marine Service (CMEMS)*. [https://doi.org/10.25423/CMCC/MEDSEA\\_ANALYSIS\\_FORECAST\\_PHY\\_006\\_013\\_EAS5](https://doi.org/10.25423/CMCC/MEDSEA_ANALYSIS_FORECAST_PHY_006_013_EAS5).
- Estournel, C., Zervakis, V., Marsaleix, P., Papadopoulos, A., Auclair, F., Perivoliotis, L., Tragou, E., 2005. Dense water formation and cascading in the Gulf of Thermaikos (North Aegean), from observations and modelling. *Continental Shelf Res.* 25 (19–20), 2366–2386.
- Falco, P., Buonocore, B., Cianelli, D., De Luca, L., Giordano, A., Iermano, I., Kalampokis, A., Saviano, S., Uttieri, M., Zambardino, G., Zambianchi, E., 2016. Dynamics and sea state in the Gulf of Naples: potential use of high-frequency radar data in an operational oceanographic context. *J. Operational Oceanograph.* 9 (Suppl. 1), s33–s45.
- Frysali, D., Mallios, Z., Theodossiou, N., 2023. Hydrologic modeling of the Aliakmon River in Greece using HEC–HMS and open data. *Euro-Mediterr. J. Environ. Integr.* 1–17.
- Genitsaris, S., Stefanidou, N., Sommer, U., Moustaka-Gouni, M., 2019. Phytoplankton blooms, red tides and mucilaginous aggregates in the urban Thessaloniki Bay, Eastern Mediterranean. *Diversity* 11 (8), 136.

- Gerritsen, H., de Goede, E.D., Platzek, F.W., van Kester, J.A.Th.M., Genseberger, M., Uittenbogaard, R.E., 2008. Validation document Delft3D-FLOW, a software system for 3D flow simulations. *Deltares* 163.
- Gotsis Skretas, O., Friligos, N., 1990. Contribution to eutrophication and phytoplankton ecology in the Thermaikos Gulf. *Thalassografika* 13, 1–12.
- Hersbach, H., Bell, B., Berrisford, P., Biavati, G., Horányi, A., Muñoz Sabater, J., Nicolas, J., Peubey, C., Radu, R., Rozum, I., Schepers, D., 2018. ERA5 Hourly Data on Single Levels from 1979 to Present, Copernicus Climate Change Service (C3S) Climate Data Store (CDS)[data set].
- Hyder, P., Simpson, J.H., Christopoulos, S., Krestenitis, Y., 2002. The seasonal cycles of stratification and circulation in the Thermaikos gulf region of freshwater influence (ROFI), north-west Aegean. *Continent. Shelf Res.* 22 (17), 2573–2597.
- Iacono, M.J., Delamere, J.S., Mlawer, E.J., Shephard, M.W., Clough, S.A., Collins, W.D., 2008. Radiative forcing by long-lived greenhouse gases: Calculations with the AER radiative transfer models. *J. Geophys. Res. Atmos.* 113 (D13).
- Janjić, Z.I., 1994. The step-mountain eta coordinate model: further developments of the convection, viscous sublayer, and turbulence closure schemes. *Mon. Weather Rev.* 122 (5), 927–945.
- Janjić, Z.I., 1996. The Surface Layer in the NCEP Eta Model. Eleventh Conference on Numerical Weather Prediction. Amer Meteor Soc, Boston, MA. Norfolk, VA; 19-23 August 1996.
- Janjić, Z.I., 2000. Comments on “Development and evaluation of a convection scheme for use in climate models”. *J. Atmos. Sci.* 57 (21), 3686–3686.
- Janjić, Z.I., 2002. Nonsingular implementation of the Mellor–Yamada level 2.5 scheme in the NCEP Meso model. NCEP Office Note 437, 61.
- Karageorgis, A.P., Skourtos, M.S., Kapsimalis, V., Kontogianni, A.D., Skoulidakis, N.T., Pagou, K., Nikolaidis, N.P., Drakopoulou, P., Zanou, B., Karamanos, H., Levkov, Z., 2005. An integrated approach to watershed management within the DPSIR framework: Axios River catchment and Thermaikos Gulf. *Reg. Environ. Change* 5 (2), 138–160.
- Kendall, M., 1975. Rank Correlation Measures, vol. 202. Charles Griffin, London, p. 15.
- Kermenidou, M., Frydas, I.S., Moschoula, E., Kousis, D., Christofilos, D., Karakitsios, S., Sarigiannis, D., 2023. Quantification and characterization of microplastics in the Thermaic gulf. In: *The North Aegean Sea. Science of The Total Environment*, 164299.
- Kourafalou, V.H., Savvidis, Y.G., Krestenitis, Y.N., Koutitas, C.G., 2004. Modelling studies on the processes that influence matter transfer on the Gulf of Thermaikos (NW Aegean Sea). *Continent. Shelf Res.* 24 (2), 203–222.
- Krestenitis, Y., Kombiadou, K., Androulidakis, Y., Makris, C., Baltikas, V., Skoulidakis, C., Kontos, Y., Kalantzi, G., 2015. Operational oceanographic platform in Thermaikos gulf (Greece): forecasting and emergency alert system for public use. In: *Proceedings of 36<sup>th</sup> International Association of Hydraulic Research (IAHR) World Congress*, The Hague, The Netherlands, 28 June – 3 July, July 2015.
- Krestenitis, Y., Pytharoulis, I., Karacostas, T.S., Androulidakis, Y., Makris, C., Kombiadou, K., Tegoulas, I., Baltikas, V., Kotsopoulos, S., Kartsios, S., 2017. Severe weather events and sea level variability over the Mediterranean Sea: the WaveForUs operational platform. In: *Perspectives on Atmospheric Sciences*, pp. 63–68.
- Krestenitis, Y.N., Androulidakis, Y., Kombiadou, K., Makris, C., Baltikas, V., Kalantzi, G., 2014. Operational oceanographic forecasts in the Thermaikos gulf: the WaveForUs project. In: *Proceedings 12<sup>th</sup> International Conference on Protection and Restoration Of the Environment (PRE)*, Skiathos Island, Greece, 29 June – 3 July 2014, pp. 313–318. ISBN 978-960-88490-6-8.
- Krestenitis, Y.N., Kombiadou, K.D., Androulidakis, Y.S., 2012. Interannual variability of the physical characteristics of north Thermaikos gulf (NW Aegean Sea). *J. Mar. Syst.* 96, 132–151.
- Krestenitis, Y.N., Kombiadou, K.D., Savvidis, Y.G., 2007. Modelling the cohesive sediment transport in the marine environment: the case of Thermaikos Gulf. *Ocean Sci.* 3 (1), 91–104.
- Krestenitis, Y., Darakas, E., Androulidakis, Y., Makris, C., Tsiridis, V., Petala, M., Antoniadou, X., Baltikas, V., Kolovoyiannis, V., Kabouraki, Z., Sakkaveli, F., Stefanidou, A., Dermetzoglou, M., 2023. Mapping of Pressures and Estimation of External and Internal Loads of Nutrients and Organic Material for the Protection and Management of the Marine Waters in Thermaikos Gulf (Thermaikos-MAPATG), Final Report. Management Authority of Thermaikos Gulf Protected Areas, p. 215 p. (in Greek).
- Kyryliuk, D., Kratzer, S., 2019. Evaluation of sentinel-3A OLCI products derived using the case-2 regional CoastColour processor over the baltic sea. *Sensors* 19 (16), 3609.
- Mann, H.B., 1945. Nonparametric tests against trend. *Econometrica: J. Econom. Soc.* 245–259.
- Mavrakis, A.F., Tsiros, I.X., 2019. The abrupt increase in the Aegean sea surface temperature during June 2007—a marine heatwave event? *Weather* 74 (6), 201–207.
- Mellor, G.L., Yamada, T., 1982. Development of a turbulence closure model for geophysical fluid problems. *Rev. Geophys.* 20 (4), 851–875.
- Morel, A., Huot, Y., Gentili, B., Werdell, P.J., Hooker, S.B., Franz, B.A., 2007. Examining the consistency of products derived from various ocean color sensors in open ocean (Case 1) waters in the perspective of a multi-sensor approach. *Rem. Sens. Environ.* 111 (1), 69–88.
- Moutzouris-Sidiris, I., Topouzelis, K., 2021. Assessment of Chlorophyll-a concentration from Sentinel-3 satellite images at the Mediterranean Sea using CMEMS open source in situ data. *Open Geosci.* 13, 85–97. <https://doi.org/10.1515/geo-2020-0204>.
- Nastos, P.T., Papadimou, K.K., Matsangouras, I.T., 2018. Mediterranean tropical-like cyclones: Impacts and composite daily means and anomalies of synoptic patterns. *Atmos. Res.* 208, 156–166.
- Novelli, G., Guigand, C.M., Cousin, C., Ryan, E.H., Laxague, N.J., Dai, H., Haus, B.K., Özgökmen, T.M., 2017. A biodegradable surface drifter for ocean sampling on a massive scale. *J. Atmos. Ocean. Technol.* 34 (11), 2509–2532.
- Pagou, K., Assimakopoulou, G., Krasakopoulou, E., Pavlidou, A., 2000. Nutrient input, fluxes and cycling in relation to the biological production in Mediterranean ecosystems influenced by river discharges: Thermaikos Gulf (Greece). In: *Dynamics of Matter Transfer and Biogeochemical Cycles: Their Modelling in Coastal Systems of the Mediterranean Sea: Final Scientific Report*, 1, pp. 50–81, 2000.
- Pytharoulis, I., Karacostas, T., Tegoulas, I., Kotsopoulos, S., Bampzelis, D., 2015a. Predictability of intense weather events over northern Greece. In: *Proceedings of 95<sup>th</sup> AMS Annual Meeting*, 4-8 January, Phoenix, Arizona, USA.
- Pytharoulis, I., Tegoulas, I., Kotsopoulos, S., Bampzelis, D., Karacostas, T., Katragkou, E., 2015b. Verification of the operational high-resolution WRF forecasts produced by WAVEFORUS project. In: *Proceedings of 16<sup>th</sup> Annual WRF Users' Workshop*, vols. 15–19. June, Boulder, Colorado, USA.
- Pytharoulis, I., Kotsopoulos, S., Tegoulas, I., Kartsios, S., Bampzelis, D., Karacostas, T., 2016. Numerical modeling of an intense precipitation event and its associated lightning activity over northern Greece. *Atmos. Res.* 169, 523–538.
- Rogers, E., Black, T., Ferrier, B., Lin, Y., Parrish, D., DiMego, G., 2001. Changes to the NCEP Meso Eta Analysis and Forecast System: Increase in Resolution, New Cloud Microphysics, Modified Precipitation Assimilation, Modified 3DVAR Analysis, vol. 488. NOAA/NWS Technical Procedures Bulletin, Washington, DC, USA. Available online: <http://www.emc.ncep.noaa.gov/mmb/mmbpl/mesoimpl/eta12tpb/>. (Accessed 24 June 2022).
- Savvidis, Y., Antoniou, A., Moriki, A., Stoilas, V.O., 2019. Downwelling events in a coastal Mussel farming area, NW Thessaloniki's gulf (NW Aegean Sea). *Ocean Sci. J.* 54 (4), 543–558.
- Simoncelli, S., Fratianni, C., Pinardi, N., Grandi, A., Drudi, M., Oddo, P., Dobricic, S., 2019. Mediterranean Sea Physical Reanalysis (CMEMS MED-Physics). Copernicus Monitoring Environment Marine Service. [https://doi.org/10.25423/MEDSEA\\_REANALYSIS\\_PHYS\\_006\\_004](https://doi.org/10.25423/MEDSEA_REANALYSIS_PHYS_006_004) (CMEMS) [Data set].
- Tran, M.C., Sentchev, A., Berti, S., Ayoub, N.K., Nguyen-Duy, T., Cuong, N.K., 2022. Assessment of relative dispersion in the Gulf of Tonkin using numerical modeling and HF radar observations of surface currents. *Continent. Shelf Res.* 245, 104784.
- Van Gils, J.A.G., Argiropoulos, D., 1991. Axios river basin water quality management. *Water Resour. Manag.* 5 (3), 271–280.
- Wang, X., Liang, X.Z., Jiang, W., Tao, Z., Wang, J.X., Liu, H., Han, Z., Liu, S., Zhang, Y., Grell, G.A., Peckham, S.E., 2010. WRF-Chem simulation of East Asian air quality: sensitivity to temporal and vertical emissions distributions. *Atmos. Environ.* 44 (5), 660–669.
- Willmott, C.J., 1981. On the validation of models. *Phys. Geogr.* 2 (2), 184–194.
- Zavattarielli, M., Mellor, G.L., 1995. A numerical study of the Mediterranean Sea circulation. *J. Phys. Oceanogr.* 25 (6), 1384–1414.
- Zervakis, V., Georgopoulos, D., 2002. Hydrology and circulation in the north Aegean (eastern Mediterranean) throughout 1997 and 1998. *Mediterr. Mar. Sci.* 3 (1), 5–19.
- Zervakis, V., Karageorgis, A.P., Kontoyiannis, H., Papadopoulos, V., Lykousis, V., 2005. Hydrology, circulation and distribution of particulate matter in Thermaikos gulf (NW Aegean Sea), during september 2001–october 2001 and february 2002. *Continent. Shelf Res.* 25 (19–20), 2332–2349.
- Zervakis, V., Kalampokis, A., Kakagiannis, G., Georgakarakos, S., Saridakis, J., 2009. Low-cost drifters for coastal use. In: *Proceedings of 9<sup>th</sup> Hellenic Symposium of Oceanography and Fisheries*, pp. 333–337.